Journal of Materials Chemistry A

REVIEW

View Article Online
View Journal | View Issue

Cite this: J. Mater. Chem. A, 2023, 11, 1061

Lignin-derived electrode materials for supercapacitor applications: progress and perspectives

Yao Tong,[a] Junyu Yang,[b] Jiajun Li,[a] Ziyang Cong,[a] Li Wei,[a] Miaomiao Liu,[a] Shangru Zhai,[a] Kai Wang *[b] and Qingda An*[a]

Received 13th September 2022
Accepted 2nd December 2022

DOI: 10.1039/d2ta07203c

rsc.li/materials-a

Lignin is one of the most abundant natural polymers and is affordable, has high carbon content and abundant active functional groups. At present, lignin-derived carbon is considered an ideal, promising electrode material for supercapacitor applications and this route is showing a vigorous development trend. In this review, we summarize the progress of lignin-derived materials for supercapacitor applications. Firstly, the concept, classification strategy and basic chemistry of lignin are introduced in brief. Then, the up-to-date developments of the synthesis strategies of carbon electrodes from lignin for supercapacitors are reviewed in detail. Finally, the work is summarized and the major challenges of the lignin-based supercapacitors are discussed. This review is presented to guide the synthesis of lignin-based electrodes for supercapacitors and facilitate their widespread application.

1. Introduction

The dwindling supply of fossil fuels and the growing demand for energy resources have stimulated the development of renewable energy and new types of energy storage devices.[1–6] Compared with other energy storage devices, supercapacitors are fascinating owing to their integrated advantages, such as high power density (>10 kW kg^{-1}), exceptionally fast charge/discharge rate (in seconds) in conjunction with an extremely long cycle life (>10^5).[7–11] Nevertheless, their subpar energy density restrains their large-scale applications; thus, one of the paramount challenges for supercapacitors is to enhance the energy density as much as possible without sacrificing the original high power density and ultra-long cycle stability.[12–14] Besides, most of the electrode materials for supercapacitor applications are extracted from unrenewable and unsustainable coal or fossil oil materials.[15–18] In this regard, the development of various renewable and sustainable resources as alternative precursors for the preparation of supercapacitors is indispensable.

Lignin is a heterogeneous and amorphous polymer. At present, approximately 70 million tons of lignin are produced during the extraction of cellulose for the paper industry each year. The affordability and bio-renewable properties make lignin a desirable candidate material for numerous applications.[19–24] Despite the huge possibilities, lignin has not yet been converted into high-value-added products on a large scale thus far.[25–28] Only a tiny percentage, approximately less than 2% of the gross product is applied as stabilizing agents,[29,30] concrete additives or surfactants and dispersants.[31–35] The rest is thrown away directly as waste or burned as low-quality fuel.[36–38] On the other hand, due to the integrated advantages of lignin, such as high carbon content, high thermal stability, biodegradability and feasible stiffness, deriving more value-added products, such as electrode materials, from lignin for supercapacitors is a potential alternative.[39–42] At present, massive efforts have already been devoted to converting lignin into carbon materials for the design of safe and reliable supercapacitors.

This review covers the recent progress in the transformation of lignin into valuable products applied in the field of supercapacitors. We shall first briefly introduce the categorization and isolation processes of lignin materials. Subsequently, the synthesis of electrode materials from lignin and their applications for supercapacitors are elaborated. Finally, the challenges and possible future directions are presented to spark new thoughts for bringing supercapacitors into practical and daily-life applications.

2. Background and isolation process of lignin

Uncovering the specific structure, categorization, source and preparation methods of various kinds of lignin is of paramount significance in investigating their potential applications. As

[a]Faculty of Light Industry and Chemical Engineering, Dalian Polytechnic University, Dalian 116034, China. E-mail: anqingda@dlpu.edu.cn
[b]Dalian National Laboratory for Clean Energy, Dalian Institute of Chemical Physics, Chinese Academy of Sciences, Dalian 116023, China. E-mail: wangkai@dicp.ac.cn

such, we will discuss the origin and fundamental structures of various kinds of lignin, as well as the isolation process.

2.1 Origin and fundamental structures of lignin

Lignin is the most abundant aromatic polymer compound in nature, which is extensively present in softwoods, hardwoods, grasses and other plants. Softwoods are comprised of the most lignin (25–35%), hardwoods are comprised of moderate lignin (20–25%), and Gramineae plants are comprised of less lignin (15–25%).[43–46] In general, lignin is chemically interwoven with hemicellulose and then wraps the outside of cellulose fibers.[47] As indicated in Fig. 1a, the bonding and strengthening between lignin, cellulose and hemicellulose play a decisive role in the strength and toughness of plant cell walls.[48]

In terms of molecular structures, lignin is an amorphous polymer with a three-dimensional network structure consisting of phenyl-propane structural units connected by ether bonds and carbon–carbon bonds.[49–52] Its phenyl-propane structural unit is usually comprised of three basic phenylpropanolic monomers, *i.e.*, sinapyl, *p*-coumaryl and coniferyl alcohols, corresponding to the three types of lignin structural units, namely, guaiacyl (G), *p*-hydrophenyl (H), and syringyl units (S), respectively (Fig. 1b).[55–58] The β-O-4′ ether linkages are the main type in lignin that account for more than 50% of the linkage structures and are certainly a critical criterion in the degradation studies.[57] The 4-O-5′, β-β′, β-5′, β-1′ and 5-5′ linkages also exist in lignin but they account for smaller percentages (Fig. 1c). The proportion of structural units and connection structures in various lignins are dissimilar depending on the plant species, growth parts, growth environment, and interference from external factors. As an example, G units constitute softwood, GS units are abundant in hardwood, while the grasses are comprised of the three monolignols, HGS-units.[23,59]

2.2 Isolation process of lignin

Lignin can be extracted from the chemical processes of pulping. The various extraction processes will affect the chemical functional groups and properties of lignin. The most crucial chemical functional groups in lignin include different numbers and proportions of hydroxyl, methoxyl, carbonyl and carboxyl groups, depending on the source of lignin and the extraction process. There are generally two strategies for separating lignin from biomass as follows: (i) polysaccharides are selectively hydrolyzed and lignin remains in the solid residues along with the decomposition products of some condensed carbohydrates;[60–62] (ii) lignin is degraded into soluble fragments and the solid residue is removed from the liquor, from which the lignin is extracted by using an appropriate solvent. At present, all the industrial pulping processes belong to the latter, resulting in the generation of technical lignin, kraft lignin, lignosulfonate and organosolv lignin.

Industrial lignin can be divided into four different types depending on whether it is subjected to the sulphuring process.[36] Kraft lignin is the dominant industrially processed lignin worldwide.[63,64] During the kraft process, the structure of pristine lignin is dramatically broken. As a consequence, kraft lignin contains more phenolic –OH groups and more condensed C–C structures.[65] Lignosulfonate is mainly derived from the waste liquid produced during the pulping process, which usually consists of active groups including phenolic hydroxyl, aliphatic hydroxyl and carbonyl. The sulfur content of lignosulfonate is rather high (*i.e.* 4–8%), most of which is in the form of sulfonate.[66,67] Organosolv lignin is derived from the by-

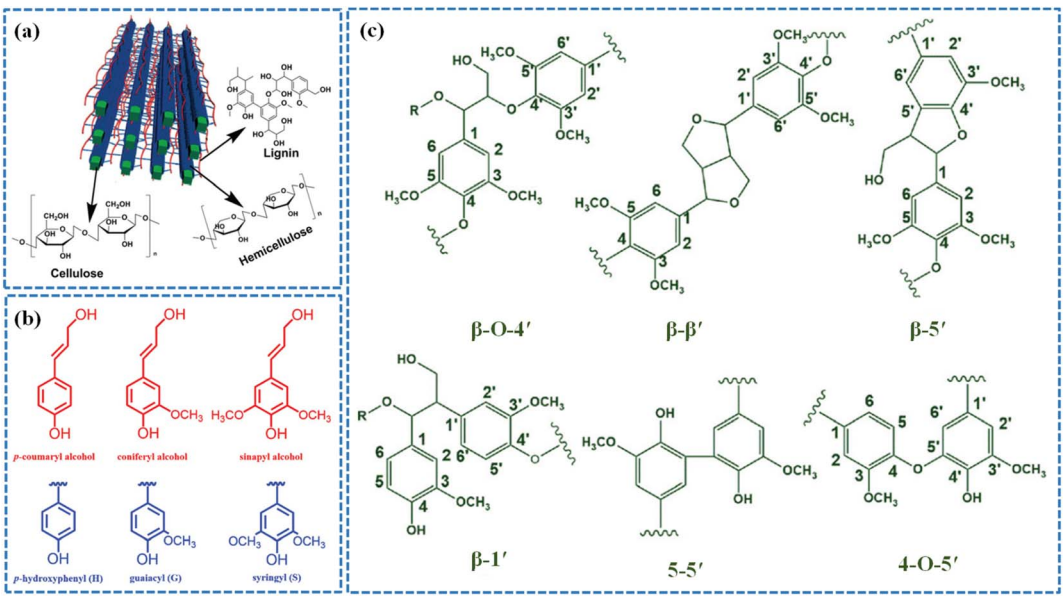

Fig. 1 (a) The natural structure of cellulose, hemicellulose and lignin in the lignocellulosic biomass. Adapted with permission from ref. 53. Copyright 2015 Royal Society of Chemistry. (b) Lignin monomer units and their precursors. (c) The linkages of lignin. Adapted with permission from ref. 54. Copyright 2017 Royal Society of Chemistry.

products of the organosolv pulping process, which exhibit smaller molecular weights and possess a higher concentration of phenolic hydroxyl groups.[36,68] Aside from these, soda lignin is mainly derived from the soda or soda–anthraquinone pulping process.[54] In comparison with kraft pulping, soda lignin has no sulfur and is more like native lignin, thus soda lignin possesses more active sites for chemical modification.[36,69] Enzymatic hydrolysis lignin is a new type of industrial lignin that is extracted from crop waste obtained during the production of bioethanol. It preserves the original lignin structure to a large extent and has higher hydrophilicity as compared to other lignin.[70,71]

3. Lignin-based electrodes for supercapacitors

Owing to their efficient, safe and reliable advantages, supercapacitors have successfully drawn extensive research interest during the past couple of decades.[72,73] Generally, supercapacitors mainly comprise electrodes, electrolytes and separators.[6,74] Among them, electrodes play a decisive role in determining the electrochemical performance of supercapacitors.[75] Supercapacitors can be normally categorized into electrical double-layer capacitors (EDLCs) and pseudo-capacitors according to their energy-storage mechanisms.[12] As shown in Fig. 2a, EDLCs rely on ion adsorption–desorption at the surface/interfaces or inner pores of electrode materials to store charges.[76,77] In recent years, a variety of carbon-based materials, such as porous carbons (PCs),[78] activated carbons (ACs),[79] carbon nanotubes (CNTs),[80] carbon aerogels (CAs),[81] carbon fibers (CFs)[82] and graphene[83] are preferred for EDLCs electrodes ascribed to their convincing merits of tunable porosity, high specific surface area (SSA), non-toxicity, superior electronic conductivity, and excellent chemical and thermal stability. Carbon-based materials can form a short electron or ion transmission distance at high energy transfer conditions, endowing EDLCs with high power density and excellent cycle stability.[84] As displayed in Fig. 2b, in comparison with EDLCs, pseudo-capacitors store energy through the reversible redox or faradaic reactions between the electrodes and electrolytes.[76] As such, pseudo-capacitors possess a higher specific capacitance and superior energy density but they suffer from lower power density and inferior cycle stability. Transition metal oxides/hydroxides and conducting polymers are typical candidates for electrode materials in pseudo-capacitors.[85] Recently, increasing attention has been devoted to the synthesis of lignin-derived carbon materials for EDLCs, benefiting from the perfect combination of the high carbon content and low-cost feature. Moreover, the quinone functional group existing in the lignin and its derivatives display strong redox activity, which is conducive to the charge transfer reactions between the electrode surface and soluble species.[86,87] Consequently, lignin and its derivatives can be utilized to prepare pseudo-capacitors as well. Table 1 summarizes in detail the recent research contributions in lignin-derived electrode materials utilized for supercapacitors.

3.1 Lignin-based electrodes for EDLCs

3.1.1 Lignin-based ACs. ACs have actuated considerable interest as a promising electrode material on account of their favorable porous structures and excellent electrical performance.[88–90] Lignin can be converted into ACs by using a physical activation or chemical activation strategy. In terms of physical activation, active agents of oxidizing gases, such as CO_2 or O_2, can etch carbon precursors at high temperatures (700–1200 °C). The generated gases escape spontaneously, leading to

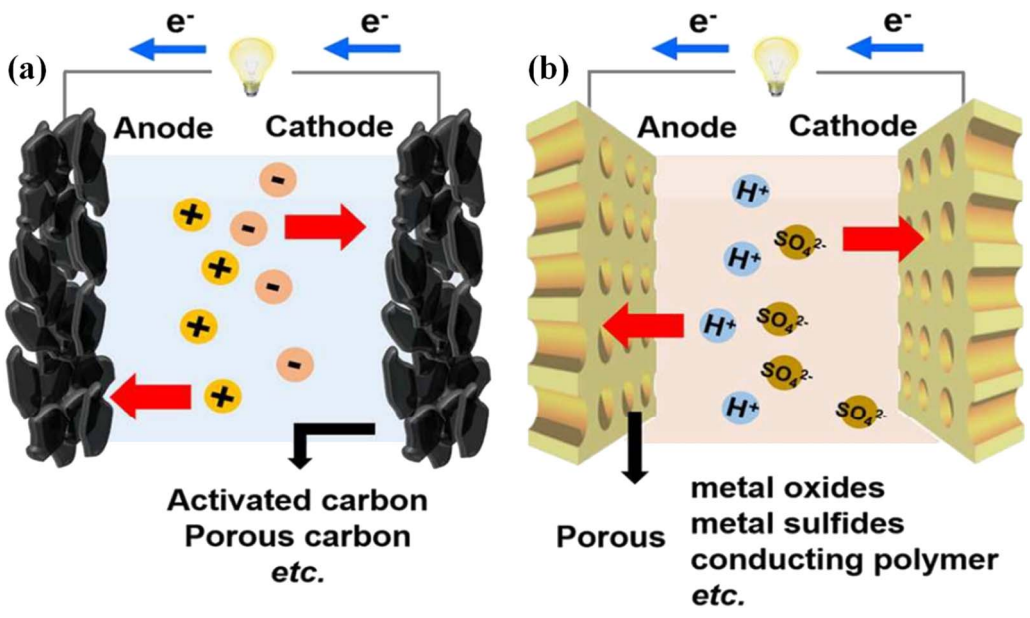

Fig. 2 Schematic diagram of (a) EDLCs and (b) pseudo-capacitors. Adapted with permission from ref. 76. Copyright 2016 Royal Society of Chemistry.

Table 1 Overview of lignin carbon-based materials in supercapacitors

Electrode materials	Structural properties	Synthesis	Electrolytes	Specific capacitance	Energy density	Cycle stability	Ref.
Lignin/PAN carbon nanofiber	S_{BET}: 1176.0 $m^2 g^{-1}$ V_t: 0.394 $cm^3 g^{-1}$	Electrospinning and self-activation process	Lignin hydrogel electrolyte	129.23 F g^{-1} at 0.5 A g^{-1} 108.90 F g^{-1} at 5 A g^{-1}	4.49 W h kg^{-1} at 2.63 kW kg^{-1}	95% after 10 000 cycles at 5 A g^{-1}	18
LFW@PANI	—	*In situ* self-polymerization	1 M H_2SO_4	800 F g^{-1} at 10 A g^{-1}	46 W h kg^{-1} at 68 kW kg^{-1}	96% after 5000 cycles at 50 mV s^{-1}	39
LCA/Ni cubic carbon	S_{BET}: 892 $m^2 g^{-1}$ V_t: 0.53 $cm^3 g^{-1}$	$ZnCl_2$ activation and template	6 M KOH	26.6 F cm^{-2} at 1 mA cm^{-2} 16.4 F cm^{-2} at 200 mA cm^{-2}	—	98.5% after 10 000 cycles at 200 mA cm^{-2}	42
HPC	S_{BET}: 1504 $m^2 g^{-1}$ V_t: 0.757 $cm^3 g^{-1}$	Hydrothermal carbonization and KOH activation	6 M KOH	324 F g^{-1} at 0.5 A g^{-1} 249 F g^{-1} at 50 A g^{-1}	17.9 W h kg^{-1} at 458 W kg^{-1}	98.07% after 5000 cycles at 5 A g^{-1}	70
HPC/WO_3	S_{BET}: 1430 $m^2 g^{-1}$ V_t: 0.41 $cm^3 g^{-1}$	Carbonization and solvothermal process	1 M H_2SO_4	432 F g^{-1} at 0.5 A g^{-1} 214 F g^{-1} at 20 A g^{-1}	34.2 W h kg^{-1} at 243 W kg^{-1}	86.6% after 10 000 cycles at 10 A g^{-1}	71
SC-1 : 1	S_{BET}: 1886 $m^2 g^{-1}$ V_t: 0.86 $cm^3 g^{-1}$	KOH activation	$EMIBF_4$	231 F g^{-1} at 1 A g^{-1} 203 F g^{-1} at 10 A g^{-1}	—	50% after 10 000 cycles at 1 A g^{-1}	91
LAC4	S_{BET}: 3775 $m^2 g^{-1}$ V_t: 2.703 $cm^3 g^{-1}$	Carbonization and KOH activation	6 M KOH	286.7 F g^{-1} at 0.2 A g^{-1} 207.1 F g^{-1} at 8 A g^{-1}	8.87 W h kg^{-1} at 51.92 W kg^{-1}	—	97
LHC-3K	S_{BET}: 1660 $m^2 g^{-1}$ V_t: 0.78 $cm^3 g^{-1}$	Hydrothermal carbonization and KOH activation	6 M KOH	420 F g^{-1} at 0.1 A g^{-1} 284 F g^{-1} at 100 A g^{-1}	10 W h kg^{-1} at 50 W kg^{-1}	99% after 5000 cycles at 5 A g^{-1}	103
PCS	S_{BET}: 1590 $m^2 g^{-1}$ V_t: 0.89 $cm^3 g^{-1}$	Spray drying; KOH activation	3 M KOH	345 F g^{-1} at 0.5 A g^{-1} 245 F g^{-1} at 10 A g^{-1}	9.7 W h kg^{-1} at 250 W kg^{-1}	94.5% after 5000 cycles at 4 A g^{-1}	198
S–PC–L-900	S_{BET}: 1054 $m^2 g^{-1}$ V_t: 1.73 $cm^3 g^{-1}$	Silica template	6 M KOH	328 F g^{-1} at 0.2 A g^{-1} 192 F g^{-1} at 20 A g^{-1}	6.9 W h kg^{-1} at 50 W kg^{-1}	94% after 10 000 cycles at 2 A g^{-1}	161
CO_2-activated mesoporous carbon from lignin	S_{BET}: 1148 $m^2 g^{-1}$ V_t: 1.00 $cm^3 g^{-1}$	Surfactant Pluronic F127/CO_2-activated	6 M KOH	102.3 F g^{-1} at 1 mVs^{-1}	—	—	107
SLC	S_{BET}: 803 $m^2 g^{-1}$ V_t: 0.86 $cm^3 g^{-1}$	Dual template of P123 and KIT-6	6 M KOH	3.0 F cm^{-2} at 0.1 A g^{-1} 1.4 F cm^{-2} at 10 A g^{-1}	0.16 mW h cm^{-2} at 1.75 mW cm^{-2}	96% after 1500 cycles at 2 A g^{-1}	109
CNSs	Thickness: 50–100 nm S_{BET}: 854.7 $m^2 g^{-1}$	Freeze-casting lignin aqueous dispersion	1 M H_2SO_4	281 F g^{-1} at 0.5 A g^{-1} 153 F g^{-1} at 20 A g^{-1}	25.1 W h kg^{-1} at 583 W kg^{-1}	91% after 5000 cycles at 1 A g^{-1}	199
LCNFs–PRL (5 : 5)	S_{BET}: 1063 $m^2 g^{-1}$ V_t: 0.53 $cm^3 g^{-1}$	Electrospinning PAN : lignin (5 : 5)	6 M KOH	339.2 F g^{-1} at 0.1 A g^{-1} 289.6 F g^{-1} at 5 A g^{-1}	56.9 W h kg^{-1} at 339 W kg^{-1} in 1 M Na_2SO_4	90.52% after 5000 cycles at 1 A g^{-1} in 1 M Na_2SO_4	112
Carbon nanofiber mats	Thickness: 50–174 μm	Electrospinning process	6 M KOH	130 F cm^{-3} at 0.1 A g^{-1} 102.7 F g^{-1} at 100 A g^{-1}	3.4 W h L^{-1} at 10 kW L^{-1}	Over 90% after 10 000 cycles at 10 A g^{-1}	116
ML-7 K CFs	S_{BET}: 2042.86 $m^2 g^{-1}$	Modification and fractionation	6 M KOH	442.2 F g^{-1} at 1 A g^{-1} 384 F g^{-1} at 10 A g^{-1}	37.1 W h kg^{-1} at 400 W kg^{-1}	97.1% after 10 000 cycles in 1 M Na_2SO_4	118

Table 1 (*Contd.*)

Electrode materials	Structural properties	Synthesis	Electrolytes	Specific capacitance	Energy density	Cycle stability	Ref.
AILCFN/Ni–Co–S	S_{BET}: 715.38 $m^2 g^{-1}$ V_t: 0.3240 mL g^{-1}	Electrospinning and thermal treatment	6 M KOH	1140.0 C g^{-1} at 10 A g^{-1}	30.8 W h kg^{-1} at 800 W kg^{-1}	84.7% after 3000 cycles at 10 mA cm^{-2}	123
K-ACFs	—	Electrospinning, carbonization and KOH activation	6 M KOH	344 F g^{-1} at 10 mv s^{-1} 196 F g^{-1} at 50 mV s^{-1}	8.1 W h kg^{-1} at 50 mV s^{-1}	96.5% after 5000 cycles	125
Lignin–cellulose-based CFs-5	S_{BET}: 837.4 $m^2 g^{-1}$ V_t: 0.488722 $cm^3 g^{-1}$	Preoxidation and carbonization treatment	6 M KOH	346.6 F g^{-1} at 0.1 A g^{-1} 285.3 F g^{-1} at 5 A g^{-1}	31.5 W h kg^{-1} at 400 W kg^{-1} in 1 M Na_2SO_4	—	126
Lignin–$NiWO_4$	—	Depositing	PVA/H_3PO_4 gel	129.7 mF cm^{-2} at 0.013 A g^{-1} 6.39 mF cm^{-2} at 0.128 A g^{-1}	2 W h cm^{-2} at 100 W cm^{-2}	84% after 2000 cycles	139
ECNF/MnO_2 (1 : 1) mat	S_{BET}: 583 $m^2 g^{-1}$ fiber diameters of ~200 nm	Electrospinning	1 M $LiPF_6$	83.3 F g^{-1} at 250 mA g^{-1}	84.3 W h kg^{-1} at 5.72 kW kg^{-1}	99% after 10 000 cycles at 2000 mA g^{-1}	142
MCNFs@SnO_2	S_{BET}: 659 $m^2 g^{-1}$	Co-electrospinning	6 M KOH	406 F g^{-1} at 0.5 A g^{-1} 128 F g^{-1} at 50 A g^{-1}	11.5 W h kg^{-1} at 451 W kg^{-1}	95% after 10 000 cycles at 10 A g^{-1}	144
LDC/ZnO	S_{BET}: 372.6 $m^2 g^{-1}$	Electrostatic self-assembling carbonization process	PVA/KOH gel	193 F g^{-1} at 0.5 A g^{-1} 151 F g^{-1} at 20 A g^{-1}	6.7 W h kg^{-1} at 197.7 W kg^{-1}	94.2% after 10 000 cycles at 2 A g^{-1}	145
PC–Ni/MnO_2-1	S_{BET}: 80.14 $m^2 g^{-1}$	Carbonization process	6 M KOH	267.34 F g^{-1} at 0.1 A g^{-1} 182.16 F g^{-1} at 2 A g^{-1}	28 W h kg^{-1} at 360 W kg^{-1}	83.6% after 5000 cycles at 1 A g^{-1}	146
KL/TAC	—	Ultrasonic-assisted deposition method	1 M H_2SO_4	293 F g^{-1} at 1 A g^{-1}	—	98.1% after 1000 cycles at 1 A g^{-1}	200
HLRGO11	S_{BET}: 1804 $m^2 g^{-1}$	Hydrothermal process	6 M KOH	190 F g^{-1} at 0.5 A g^{-1} 133.9 F g^{-1} at 10 A g^{-1}	—	86.5% after 10 000 cycles at 10 A g^{-1}	133
Lig–GHs	S_{BET}: 109 $m^2 g^{-1}$	Hydrothermal process	0.1 M $HClO_4$	549.5 F g^{-1} at 1 A g^{-1} 335 F g^{-1} at 20 A g^{-1}	—	83.7% after 1000 cycles at 20 A g^{-1}	132
C–LRGOs	S_{BET}: 444.29 $m^2 g^{-1}$ V_t: 0.773 $cm^3 g^{-1}$	Hydrothermal reaction and carbonization	1 M H_2SO_4	330 F g^{-1} at 1 A g^{-1} 265 F g^{-1}at 10 A g^{-1}	11.3 W h kg^{-1} at 254 W kg^{-1}	100% after 10 000 cycles at 50 mV s^{-1}	134
HPCSLS-700-1	S_{BET}: 903 $m^2 g^{-1}$ V_t: 0.53 $cm^3 g^{-1}$	Direct carbonization	7 M KOH	247 F g^{-1} at 0.05 A g^{-1} 104 F g^{-1} at 20 A g^{-1}	8.6 W h kg^{-1} at 14.3 W kg^{-1}	92% after 10 000 cycles at 2 A g^{-1}	162
$NHPC_{1:1}$-3-800	S_{BET}: 1867.4 $m^2 g^{-1}$ V_t: 0.997 $cm^3 g^{-1}$	Hydrothermal crosslinking reaction and KOH activation	6 M KOH 1 M H_2SO_4	440 F g^{-1} at 0.5 A g^{-1} 331 F g^{-1} at 1 A g^{-1}	18.5 W h kg^{-1} at 300 W kg^{-1} in 6 M KOH	95.1% after 3000 cycles at 20 A g^{-1} in 6 M KOH	163
N, S–HPC-1	S_{BET}: 1454.7 $m^2 g^{-1}$ V_t: 0.894 $cm^3 g^{-1}$	Carbonization and KOH activation	6 M KOH	269 F g^{-1} at 0.5 A g^{-1} 168 F g^{-1} at 50 A g^{-1}	37.4 W h kg^{-1} at 62 W kg^{-1}	98.4% after 10 000 cycles at 5 A g^{-1}	164
L–U	S_{BET}: 3130 $m^2 g^{-1}$ V_t: 1.67 $cm^3 g^{-1}$	Carbonization and KOH activation	KOH–PVA	306 F g^{-1} at 0.1 A g^{-1} 251 F g^{-1} at 10 A g^{-1}	17 W h kg^{-1}	96.8% after 5000 cycles at 0.1 to 10 A g^{-1}	172
PL-700	S_{BET}: 2265 $m^2 g^{-1}$	KOH activation	6 M KOH	333 F g^{-1} at 20 mV s^{-1}	—	100% after 1000 cycles at 1 A g^{-1}	173

Table 1 (*Contd.*)

Electrode materials	Structural properties	Synthesis	Electrolytes	Specific capacitance	Energy density	Cycle stability	Ref.
GNs–N–S co-doped ACNFs-5	S_{BET}: 2439 m^2 g^{-1} V_t: 1.2882 cm^3 g^{-1}	Electrospinning, carbonization and activation process	6 M KOH	267.32 F g^{-1} at 5 mV s^{-1} 148.47 F g^{-1} at 50 mV s^{-1}	9.28 W h kg^{-1} at 493 W kg^{-1}	96.7% after 5000 cycles	175
ONS–HPCs–L-700	S_{BET}: 1269 m^2 g^{-1} V_t: 0.598 cm^3 g^{-1}	Direct pyrolysis	6 M KOH	300.5 F g^{-1} at 0.5 A g^{-1} 243 F g^{-1} at 60 A g^{-1}	66.8 W h kg^{-1} at 1750 W kg^{-1} in EMIM BF4	91.6% after 10 000 cycles at 5 A g^{-1} in 6 M KOH	180
CKL-1098	S_{BET}: 1092 m^2 g^{-1}	Direct carbonization	1 M H_2SO_4	114 F g^{-1} at 5 mV s^{-1} 76 F g^{-1} at 100 mV s^{-1}	12.8 W h kg^{-1} at 1006 W kg^{-1}	80% after 10 000 cycles at 50 mV s^{-1}	201
Ca-800	S_{BET}: 1362 m^2 g^{-1} V_t: 0.83 cm^3 g^{-1}	Carbonization	6 M KOH	182 F g^{-1} at 1 mA cm^{-2} 122 F g^{-1} at 20 mA cm^{-2}	25 W h kg^{-1} at 150 W kg^{-1}	95% after 1000 cycles at 10 mA cm^{-2}	202
CHMS-5-700–N	S_{BET}: 991 m^2 g^{-1} V_t: 0.75 cm^3 g^{-1}	Carbonization and post-nitric acid modification	7 M KOH	284 F g^{-1} at 0.1 A g^{-1} 124 F g^{-1} at 20 A g^{-1}	2.9 W h L^{-1} at 11.3 W L^{-1}	93.4% after 10 000 cycles at 2 A g^{-1}	203
HPCS-700	S_{BET}: 1255 m^2 g^{-1} V_t: 0.87 cm^3 g^{-1}	Thermostabilization and carbonization	7 M KOH	276 F g^{-1} at 0.1 A g^{-1} 155 F g^{-1} at 20 A g^{-1}	34.3 W h kg^{-1} at 9.4 kW kg^{-1} in 1 M SBPBF4/PC	99.5% after 10 000 cycles at 2 A g^{-1}	204
HAPC-11-900	S_{BET}: 856 m^2 g^{-1} V_t: 0.17 cm^3 g^{-1}	Template and chemical activation	6 M KOH	286 F g^{-1} at 0.25 A g^{-1} 141 F g^{-1} at 10 A g^{-1}	13 W h kg^{-1} at 27 kW kg^{-1}	89.4% after 2000 cycles at 4 A g^{-1}	205
PNG	S_{BET}: 515 m^2 g^{-1}	Co-pyrolysis	6 M KOH	170 F g^{-1} at 0.2 A g^{-1} 138.5 F g^{-1} at 5 A g^{-1}	—	92.5% after 1000 cycles at 100 mV s^{-1}	206
HPGC-160-8	S_{BET}: 856.84 m^2 g^{-1} V_t: 0.425 cm^3 g^{-1}	Cross-linking and carbonization	6 M KOH	331 F g^{-1} at 5 mV s^{-1} 202 F g^{-1} at 100 mV s^{-1}	—	78% after 1000 cycles at 20 mV^{-1}	207
LHPC	S_{BET}: 907 m^2 g^{-1} V_t: 0.515 cm^3 g^{-1}	Template-free and KOH activation	1 M H_2SO_4	165 F g^{-1} at 0.05 A g^{-1} 123.5 F g^{-1} at 10 A g^{-1}	3.75 W h kg^{-1} at 1070 W kg^{-1}	97.45% after 5000 cycles at 1 A g^{-1}	208
NiO/HMPC NSs	S_{BET}: 851.8 m^2 g^{-1} V_t: 0.16 cm^3 g^{-1}	Self-assembly and carbonization	6 M KOH	508 F g^{-1} at 20 mV s^{-1}	—	92% after 2000 cycles at 20 mV s^{-1}	209
1-$HPC_{600\text{-}600\text{-}5}$	S_{BET}: 2753.9 m^2 g^{-1} V_t: 1.43 cm^3 g^{-1}	Carbonization and KOH activation	6 M KOH	428 F g^{-1} at 0.04 A g^{-1} 288 F g^{-1} at 10 A g^{-1}	12 W h kg^{-1} at 9908 W kg^{-1}	96% after 12 000 cycles at 5 A g^{-1}	210
CA-L20	S_{BET}: 779 m^2 g^{-1} V_t: 0.48 cm^3 g^{-1}	Carbonization and KOH activation	6 M KOH	142.8 F g^{-1} at 0.5 A g^{-1} 112.5 F g^{-1} at 10 A g^{-1}	—	96% after 2000 cycles at 10 A g^{-1}	211
PANI/LGS	—	—	1 M H_2SO4	502.1 F g^{-1} at 0.1 A g^{-1} 377.2 F g^{-1} at 10 A g^{-1}	—	74.3% after 10 000 cycles at 1 A g^{-1}	212
PANI/LG	—	*In situ* oxidation polymerization	1 M $HClO_4$	485.3 F g^{-1} at 0.5 A g^{-1} 284.4 F g^{-1} at 30 A g^{-1}	—	67.4% after 5000 cycles at 1 A g^{-1}	213
ECNFs (70/30)	S_{BET}: 583 m^2 g^{-1} V_t: 0.289 cm^3 g^{-1}	Electrospinning, stabilization and carbonization	6 M KOH	64 F g^{-1} at 0.4 A g^{-1} 50 F g^{-1} at 2 A g^{-1}	5.67 W h kg^{-1} at 94.19 W kg^{-1}	90% after 6000 cycles at 2 A g^{-1}	214

Table 1 (*Contd.*)

Electrode materials	Structural properties	Synthesis	Electrolytes	Specific capacitance	Energy density	Cycle stability	Ref.
$NiCo_2O_4$@CNF55	Fiber diameters of 1830 ± 155 nm	Electrospinning, stabilization and carbonization	2 M KOH	1757 F g^{-1} at 2 mA cm^{-2} 1304 F g^{-1} at 50 mA cm^{-2}	47.75 W h kg^{-1} at 799.53 W kg^{-1}	138% after 5000 cycles at 7 mA cm^{-2}	215
LCNFs-2	S_{BET}: 1140 m^2 g^{-1} V_t: 0.627 cm^3 g^{-1}	Electrospinning PVP : $Mg(NO_3)_2 \cdot 6H_2O$: lignin (2 : 2 : 1)	6 M KOH	248 F g^{-1} at 0.2 A g^{-1} 146 F g^{-1} at 20A g^{-1}	—	97% after 1000 cycles at 20 A g^{-1}	216
MnO_2–CNFM4	—	Electrospinning, carbonization	1 M Na_2SO_4	171.6 F g^{-1} at 5 mV?s^{-1} 88.4 F g^{-1} at 50 mV s^{-1}	6.0 W h kg^{-1} at 160 W kg^{-1}	98.95% after 1000 cycles at 0.5 A g^{-1}	217
MnO_2–LCF-800 mat	S_{BET}: 273.70 m^2 g^{-1} V_t: 0.09 cm^3 g^{-1}	Electrospinning, stabilization and carbonization	1 M Na_2SO_4	131.28 F g^{-1} at 0.3 A g^{-1}	14.77 W h kg^{-1} at 135.01 W kg^{-1}	—	218
LUDC_0.5	S_{BET}: 764 m^2 g^{-1} V_t: 0.47 cm^3 g^{-1}	DES-templated	6 M KOH	177.5 F g^{-1} at 0.5 A g^{-1} 136.8 F g^{-1} at 10 A g^{-1}	—	96% after 12 000 cycles at 10 A g^{-1}	219
BALC-9	S_{BET}: 1831 m^2 g^{-1} V_t: 1.53 cm^3 g^{-1}	Carbonization and bacterial activation	6 M KOH EMIM TFSI	428 F g^{-1} at 1 A g^{-1} 289 F g^{-1}at 1 A g^{-1}	66.18 W h kg^{-1} at 312 W kg^{-1} in EMIM TFSI	96.7% after 10 000 cycles at 5 A g^{-1} in 6 M KOH	104
ARS/PGLS-1	S_{BET}: 1727.7 m^2 g^{-1} V_t: 1.33 cm^3 g^{-1}	Carbonization and graphitization	6 M KOH	469.5 F g^{-1} at 0.5 A g^{-1} 200.2 F g^{-1} at 10 A g^{-1}	9.45 W h kg^{-1} at 100.06 W kg^{-1} in PVA/KOH/ARS	99.7% after 2000 cycles at 2 A g^{-1} in PVA/KOH/ARS	220
LSG-P36–Au	S_{BET}: 338.3 m^2 g^{-1} V_t: 0.232 cm^3 g^{-1}	One-step CO_2 laser irradiation	H_2SO_4/PVA gel	11.9 mF cm^{-2} at 0.02 mA cm^{-2}	—	98.47% after 12 000 cycles at 2 mA cm^{-2}	221
sLIG-O/S14	S_{BET}: 181.37 m^2 g^{-1} V_t: 0.351 cm^3 g^{-1}	A duplicated laser scribing process	PVA/H2SO4 gel	53.2 mF cm^{-2} at 0.08 mA cm^{-2}	0.45 mW h cm^{-3} at 1.6 mW cm^{-2}	81.3% after 8000 cycles at 50 mV s^{-1}	222
N–BLPC	S_{BET}: 2646 m^2 g^{-1} V_t: 1.285 cm^3 g^{-1}	KOH activation	6 M KOH	337 F g^{-1} at 0.5 A g^{-1} 254 F g^{-1} at 20 A g^{-1}	9.34 W h kg^{-1} at 250 W kg^{-1}	98% after 3000 cycles at 10 A g^{-1}	223
LPC-3	S_{BET}: 2866 m^2 g^{-1} V_t: 2.02 cm^3 g^{-1}	Microwave heating	6 M KOH	216 F g^{-1} at 0.5 A g^{-1} 188 F g^{-1} at 10 A g^{-1}	55.5 W h kg^{-1} at 1.1 kW kg^{-1}	99.9% after 2000 cycles at 5 A g^{-1} in gel-like PVA/LiCl electrolyte	224
NSC-700	S_{BET}: 1199 m^2 g^{-1}	Fe_3O_4 template and KOH activation	6 M KOH	241 F g^{-1} at 1 A g^{-1} 196 F g^{-1} at 20 A g^{-1}	27.2 W h kg^{-1} at 10 000 W kg^{-1}	95% after 3000 cycles at 10 A g^{-1}	225
E-CNFs	S_{BET}: 2313 m^2 g^{-1}	Esterification, electrospinning, and carbonization processes	6 M KOH	320 F g^{-1} at 1 A g^{-1} 200.4 F g^{-1} at 20 A g^{-1}	17.92 W h kg^{-1} at 800 W kg^{-1} in 1 M Na_2SO_4	94.5% after 5000 cycles at 1 A g^{-1} in 1 M Na_2SO_4	226
LUPCF-2	S_{BET}: 1363 m^2 g^{-1} V_t: 0.689 cm^3 g^{-1}	Electrospinning, pre-oxidation, carbonization, and pickling processes	6 M KOH	289 F g^{-1} at 0.1 A g^{-1} 162 F g^{-1} at 20 A g^{-1}	—	92% after 10 000 cycles at 5 A g^{-1}	227
PLC-650-2	S_{BET}: 1069 m^2 g^{-1} V_t: 1.375 cm^3 g^{-1}	Zinc oxalate-assisted gas-exfoliation and *in situ* templating	6 M KOH	365 F g^{-1} at 0.5 A g^{-1} 260 F g^{-1} at 20 A g^{-1}	9.75 W h kg^{-1} at 6157.9 W kg^{-1} in PVA/KOH gel electrolytes	93.5% after 10 000 cycles at 5 A g^{-1}	105
CNFs-6	S_{BET}: 1061.7 m^2 g^{-1} V_t: 0.57 cm^3 g^{-1}	ECH modification and heat treatment	6 M KOH	320.3 F g^{-1} at 1 A g^{-1}	30.2 W h kg^{-1} at 400 W kg^{-1} in 1 M Na_2SO_4	—	228
L–CNFs@Fe_3O_4 nanofibers	—	Electrospinning, stabilized and carbonized	1 M Na_2SO_4	216 F g^{-1} at 0.1 A g^{-1}	43 W h kg^{-1} at 242 W kg^{-1}	96.7% after 1000 cycles at 1 A g^{-1}	229

Table 1 (*Contd.*)

Electrode materials	Structural properties	Synthesis	Electrolytes	Specific capacitance	Energy density	Cycle stability	Ref.
C800-SS	S_{BET}: 28.3 m^2 g^{-1} V_t: 0.068 cm^3 g^{-1}	Electrospinning and carbonization	PVA-1 M H_2SO_4	451.1 F g^{-1} at 1 A g^{-1}	62.6 W h kg^{-1} at 1250 W kg^{-1}	99.5% after 10 000 cycles	230
HPCS-X-3	S_{BET}: 3406 m^2 g^{-1} V_t: 2.46 cm^3 g^{-1}	Simple spray drying and carbonization-activation	6 M KOH	236.2 F g^{-1} at 0.2 A g^{-1} 130.6 F g^{-1} at 20 A g^{-1}	—	91.7% after 5000 cycles at 20 A g^{-1}	231
LPC-700	S_{BET}: 529 m^2 g^{-1}	Carbonization-induced self-template method	6 M KOH	170 F g^{-1} at 0.5 A g^{-1} 89 F g^{-1}at 10 A g^{-1}	—	81% after 5000 cycles at 1 A g^{-1}	232
NCA-12	S_{BET}: 482 m^2 g^{-1}	Co-electrospinning, freeze-casting and freeze-drying, carbonization	6 M KOH	282 F g^{-1} at 0.2 A g^{-1} 60 F g^{-1} at 10 A g^{-1}	32 W h kg^{-1} at 125 W kg^{-1}	96% after 5000 cycles at 5 A g^{-1}	233
LPCs	S_{BET}: 3178.36 m^2 g^{-1}	Hydrothermal and KOH-assisted synthesis	6 M KOH	201.69 F g^{-1} at 0.5 A g^{-1} 171.88 g^{-1} at 10 A g^{-1}	—	90.21% after 10 000 cycles at 10 A g^{-1}	234
LCNS	S_{BET}: 736 m^2 g^{-1}	Self-assembly, stabilization treatment, and carbonization	6 M KOH	147 F g^{-1} 0.5 A g^{-1} 86 F g^{-1} at 20 A g^{-1}	3.5 W h kg^{-1} at 62.6 W kg^{-1}	85.37% after 10 000 cycles at 10 A g^{-1}	235
LSC–ZnC_2O_4/PANI	—	Carbonization and *in situ* polymerization	1 M H_2SO_4	643 F g^{-1} at 1.0 A g^{-1} 390 F g^{-1} at 30 A g^{-1}	36.3 W h kg^{-1} at 850.2 W kg^{-1} in 1 M Na_2SO_4	88.0% after 5000 cycles at 5.0 A g^{-1}	236

the formation of small and well-developed pore structures on the surface and inside of the carbonized materials.[41,91] As for the chemical activation, lignin-based carbons are initially mixed with chemical active agents (such as KOH, $ZnCl_2$, K_2CO_3, Na_2CO_3, H_3PO_4, *etc.*); subsequently, the mixture is heated at low temperature (400–700 °C) in an inert atmosphere.[92–96] Various cross-linking and polycondensation reactions occur between lignin and chemical activators, which release carbon, hydrogen and oxygen atoms from the lignin, resulting in a large number of multi-scale pores. In particular, the chemical activation results in stronger pore-forming ability and takes place at lower temperatures in comparison with the physical activation, thereby making it the main approach for the synthesis of lignin-based ACs with large SSA.[41,51] Zhang *et al.* studied the influence of preparation conditions on the structures and properties of lignin-derived ACs *via* the KOH-activation strategy.[97] They found that the increment of activation temperature and KOH/carbon ratio improved the SSA of ACs. Nevertheless, the excessively high activation temperature could destroy the pores, leading to decreased SSA and capacitance. Eventually, the electrode activated at 800 °C with a KOH/carbon ratio of 4 : 1 displayed the champion SSA of 3775 m^2 g^{-1}, and delivered a considerable specific capacitance of 286.7 F g^{-1} at 0.2 A g^{-1} in 6 M KOH.

Of special note, the activator plays a paramount role in the ultimate SSA and pore structure of the lignin-based carbon materials. Wu *et al.* demonstrated that the electrochemical performance of lignin-based ACs depends on the various activators ($ZnCl_2$, KOH, K_2CO_3).[98] Interestingly, the $ZnCl_2$-activated ACs exhibited the smallest SSA because $ZnCl_2$ only acts as a catalyst for dehydroxylation and dehydration in the activation process, whereas both KOH and K_2CO_3 serve to dehydrate and oxidize lignin. Furthermore, K_2CO_3 decomposes into CO_2 and introduces physical activation. As such, the K_2CO_3-activated ACs exhibited the maximum SSA of 1585 m^2 g^{-1} and an excellent specific capacitance of 263.5 F g^{-1} at 40 mA g^{-1} in 6 M KOH.

A high SSA is of significance for raising the performance of lignin-based ACs, but a suitable pore structure is a prerequisite to the high utilization of the SSA.[99] For example, most high SSA materials are usually microporous with a narrow pore size distribution of 0.5–1.5 nm, which severely restrains the diffusion of electrolyte ions, and undermines the rate capability.[100–102] To tackle these issues, hierarchical porous carbons (HPCs) combining micro-, meso- and macro-pores have been utilized as EDLCs electrode materials as they are capable of offering effective diffusion paths. In HPCs, the macropores provide a high buffer capacity for electrolyte ions, the mesoporous channels are conducive to the rapid transport of ions, and the micropores can further enhance the ion-accessible surface area for the construction of an electric double layer, resulting in excellent electrochemical performance.[101] Lignins enjoy a loose structure that is conducive to the formation of porous structures during pyrolysis. In this regard, tremendous efforts have been devoted to constructing HPCs *via* appropriate pyrolysis and activation strategies by adopting lignin as a carbon source. Guo and co-workers configured a 3D HPC from

the enzymatic hydrolysis of lignin *via* hydrothermal carbonization followed by a KOH activation process (Fig. 3a).[103] The unique 3D porous network (Fig. 3b) exhibited a high SSA of 1660 $m^2 g^{-1}$ and realized a superior specific capacitance of 420 F g^{-1} at 0.1 A g^{-1}, together with considerable rate performance in 6 M KOH (Fig. 3c). Moreover, it can retain 99% of the pristine capacitance upon undergoing 10 000 cycles at 5 A g^{-1}, indicative of excellent structural stability. Strikingly, the assembled symmetric supercapacitor exhibited an outstanding energy density of 46.8 W h kg^{-1} in ionic liquid systems (Fig. 3d). Based on this work, our group systematically studied the effects of hydrothermal carbonization conditions on the structure and properties of HPCs according to the Taguchi method.[70] The optimized sample enjoyed a favorable SSA of 1504 $m^2 g^{-1}$ and the corresponding supercapacitors delivered a desirable specific capacitance of 324 F g^{-1} at 0.5 A g^{-1} in 6 M KOH coupled with decent rate performance and excellent cycle stability. Zhang *et al.* developed a green bacterial activation strategy to prepare HPCs.[104] It is worth noting that bacterial activation can break the β-O-4, β-β′, and β-5 linkages in lignin, reduce the molecular weight, and promote the carbonization and graphitization of lignin. As such, an enhanced specific capacitance of 428 F g^{-1} at 1 A g^{-1} in 6 M KOH was achieved. In addition, the symmetric supercapacitor can deliver a superior energy density of 66.18 W h kg^{-1} at a power density of 312 W kg^{-1} in the ionic liquid system. It also achieved a decent cycle performance, with a capacitance retention of up to 96.7% after 10 000 cycles at 5 A g^{-1}.

3.1.2 Templated carbon. To enhance the electrochemical properties, the templating method, utilizing hard templates (magnesium-based, silica-based, zinc-based and calcium-based templates), soft templates (conventional soft template, ionic liquids, deep eutectic solvent) or self-templates (biomass, MOFs), has been performed to prepare PCs with well-built pore structures and pore size distributions.[42,72,92,104,105] In the synthesis of hard template carbon, templates are initially incorporated into the lignin matrix, and then the templates are carbonized and removed by utilizing chemical or physical methods. As such, the templated electrodes have uniform mesopores that can provide fast-moving channels for electrolyte ions and endow excellent rate performance for supercapacitors. Rosas *et al.* configured HPCs from lignin by adopting Y and β zeolites as hard templates.[106] Intriguingly, these formed carbons feature abundant surface oxygen groups, accompanied by pyridone and pyridinic groups. Thus, the supercapacitor based on the HPCs delivered an improved specific capacitance of 250 F g^{-1} at 50 mA g^{-1} in 1 M H_2SO_4, with a capacitance retention of 50% after 20 000 cycles and a volumetric capacitance of 75 F cm^{-3} at 20 A g^{-1}.

However, the synthesis and removal of the hard template are complicated, and the properties of PCs largely depend on the properties of templates. Recently, the soft template method has attracted much more attention because it is unnecessary to remove the soft templates after carbonization. The soft template and abundant oxygen-containing functional groups in lignin can self-assemble into precursors through hydrogen bond interactions, and the mesoporous materials can be synthesized by subsequently carbonizing the precursors. Saha *et al.*[107] prepared lignin-based ordered mesoporous carbons (OMCs) by adopting Pluronic F127 as the template. The OMCs showed an SSA of 1148 $m^2 g^{-1}$, with a mesoporosity of 66%. The OMCs electrode activated by CO_2 delivered a capacitance of 102.3 F g^{-1} and excellent rate performance in 6 M KOH. Moreover, Herou *et al.*[108] adopted the dual precursor system comprising equal-weight phloroglucinol and lignin to prepare OMCs through a soft template strategy. The synthesized OMCs displayed

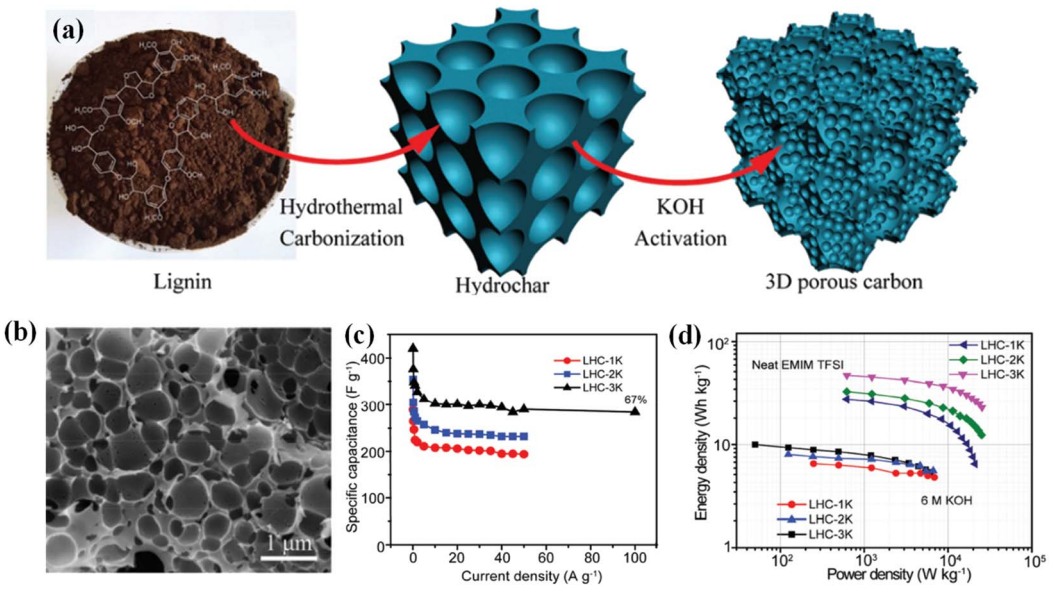

Fig. 3 (a) Schematic of the synthesis of LHC samples. (b) SEM image of the LHC-3K. (c) Rate performance of the LHC-based electrodes. (d) Ragone profiles of LHC-based supercapacitors (LHC denoted as enzymatic hydrolysis lignin-derived 3D HPCs). Reproduced with permission from ref. 103. Copyright 2017 Royal Society of Chemistry.

superior electrochemical performance as compared to the material prepared by only utilizing phloroglucinol because the smaller mesopores in the former boosted the electrolyte diffusion rate.

Compared with the hard template method, the soft template method shows an underdeveloped capability of selectively regulating the pore structure of PCs and thus, the prepared PCs possess fewer micropores and smaller SSA. With the above information in mind, an efficient strategy is to couple the hard template with the soft template method to achieve carbon electrodes possessing appropriate pore structures. Li *et al.* configured large-scale hierarchical porous carbon monoliths (HPCMs), by effectively carbonizing the mixture of P123, lignin and mesoporous silica (hereafter denoted as SLC), as shown in Fig. 4a.[109] The SLC displays a favorable microstructure and excellent conductivity. As expected, the assembled symmetric supercapacitor exhibited a superior areal capacity of 3.0 F cm^{-2} and a volume capacity of 97.1 F cm^{-3} at a current density of 1.4 mA cm^{-2} in 6 M KOH without utilizing binders and conductive additives (Fig. 4b). Moreover, a considerable areal energy density of 0.16 mW h cm^{-2} at 1.75 mW cm^{-2} was achieved (Fig. 4c). In another study, Song *et al.* constructed the mesostructured carbons by employing MgO and Pluronic F127 as templates. They revealed that both the space-occupying effect of the MgO template and the mass ratio of lignin/MgO are critical for regulating the porosity of carbons. Eventually, the obtained material achieved a high SSA of 712 m^2 g^{-1} and the fabricated electrodes yielded a larger specific capacitance of 186.3 F g^{-1} at a current density of 0.1 A g^{-1} in 1 M H_2SO_4.[111]

Recent studies have demonstrated that the templates not only construct pores but also play other roles in the preparation of lignin-based carbon materials.[110] As illustrated in Fig. 4d, Wang and coworkers reported an inverse phase dehydration method to effectively synthesize the HPCMs.[110] In this work, K_2CO_3 firstly acts as a pH regulator to promote the dissolution of lignin, and subsequently serves as the mesopore template and activator to promote the formation of abundant micropores of approximately 4 nm (Fig. 4e). The supercapacitor fabricated based on the optimal sample (HPCM-0.75) delivered a remarkable capacitance of 140 F g^{-1} at 0.05 A g^{-1} and excellent rate performance where the electrolyte used was 1 M tetraethylammonium tetrafluoroborate salt solution in propylene carbonate (Fig. 4f).

3.1.3 Electrospinning CFs. In recent years, CFs have been regarded as ideal electrode materials used in supercapacitors.[112–117] Electrospinning technology provides a convenient approach to producing continuous nanofibers with favorable SSA and uniform diameters on a scale ranging from sub-micrometers to a few nanometers. Subsequently, the spun nanofibers can be transformed into CFs with features of uniform pore distribution and superior mechanical properties *via* the stabilization and carbonization processes.[118–123] Jayawickramage *et al.* successfully synthesized polyacrylonitrile (PAN)/lignin hybrid CFs by electrospinning, which were subsequently subjected to thermal stabilization, carbonization and CO_2 activation.[124] The obtained CF electrode displayed a high SSA (2370 m^2 g^{-1}), in conjunction with excellent mesoporosity and favorable electrical conductivity. Moreover, the fabricated coin cell supercapacitor delivered an outstanding specific capacitance of 128 F g^{-1} in the ionic liquid electrolyte. An energy density of 59 W h kg^{-1} at a power density of 15 kW kg^{-1} was also achieved. Hu and coworkers achieved the transition from rather hydrophobic CFs to hydrophilic and readily water-wettable activated carbon fibers (ACFs) through a NaOH (Na-ACFs) and KOH (K-ACFs) activation process.[125] The obtained ACFs possess large basal plane sizes and excellent electrical

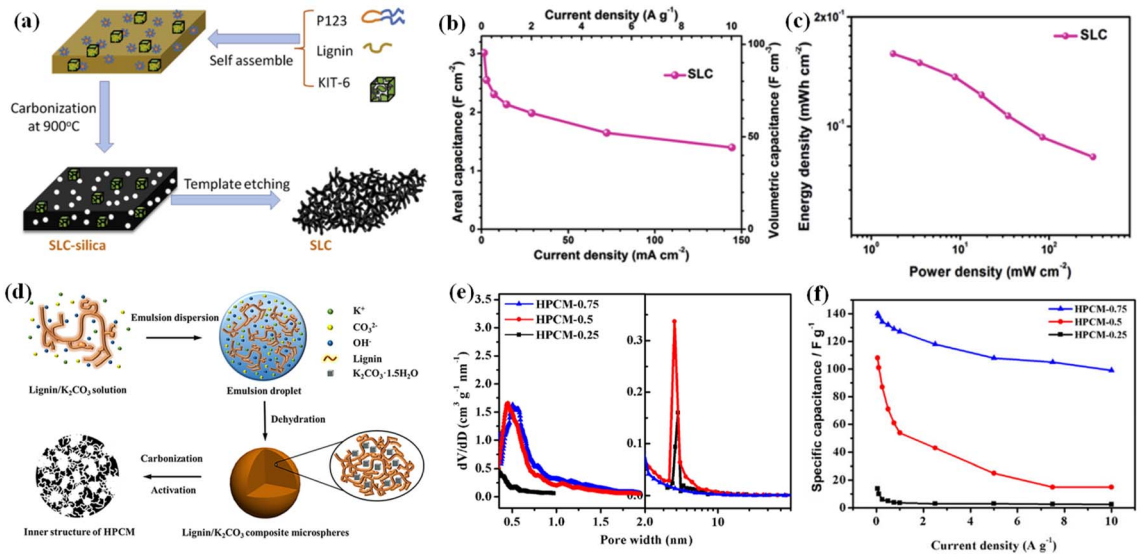

Fig. 4 (a) Schematic illustration of the SLC process. (b) Areal/volumetric capacitances of SLC. (c) Areal Ragone plots (energy density *vs.* power density) for the full cell. Reprinted with permission from ref. 109. Copyright 2016 Elsevier. (d) Schematic of the formation of lignin/K_2CO_3 composite microspheres. (e) Micropore and mesopore size distribution of HPCMs. (f) The rate performance of various HPCMs at different scan rates. Reprinted with permission from ref. 110. Copyright 2018 Wiley Online Library.

conductivity, thus giving rise to outstanding electrochemical performance (Fig. 5a). In particular, K-ACFs showed a superior specific capacitance of 344 F g^{-1} at 10 mV s^{-1} in 6 M KOH as compared to Na-ACFs due to the higher microporosity and more narrowly distributed pore size of the former (Fig. 5b).

The low molecular weight, high heterogeneity and large dispersion index of lignin hinder the preparation of high-quality CFs from pure lignin.[118,127] Zhou and coworkers utilized the reaction between the hydroxyl groups in lignin and the isocyanate groups in isophorone diisocyanate to enhance the molecular weight and reduce the heterogeneity of lignin, thus decreasing the carbon weight loss of precursor fibers and maintaining the morphology of lignin-based CFs.[118] Correspondingly, the prepared CFs exhibited an outstanding SSA of 2042.86 m^2 g^{-1}. The assembled optimized supercapacitors displayed a high specific capacitance of 428.9 F g^{-1} at 1 A g^{-1} in 6 M KOH. Also, an excellent energy density of 37.1 W h kg^{-1} at a power density of 400 W kg^{-1} was realized in 1 M Na_2SO_4 electrolyte. In another study, Cao and co-workers modified lignin with cellulose-acetate to obtain precursor fibers by employing a facile phosphating process (Fig. 5c).[126] Thereafter, lignin-based CFs were subjected to pre-oxidizing and carbonizing processes, thereby obtaining electrodes with high SSA and excellent electrochemical performance. Accordingly, the fabricated supercapacitor exhibited a capacitance of up to 346.6 F g^{-1} at 0.1 A g^{-1} in 6 M KOH. A superior energy density of 31.5 W h kg^{-1} at a power density of 400 W kg^{-1} was achieved in 1 M Na_2SO_4 electrolyte as well. Notably, the energy density of the supercapacitor was astonishingly maintained at 24.3 W kg^{-1} when the power density increased to 4000 W kg^{-1}.

3.1.4 Graphene/lignin composite. Graphene has attracted considerable interest in supercapacitors because of its large SSA, high electrical conductivity and excellent chemical stability. Nonetheless, single-layer graphene tends to restack due to strong van der Waals interactions, which severely decreases the accessible area, thereby greatly restricting the mass transport process.[128,129] Lignin comprises phenylpropanoid subunits in a 3D spatial structure, which attenuates the restacking π–π interaction effect of graphene. Thus, combining lignin with graphene is a remedy that makes full use of graphene's advantages and enhances the performance of lignin-based electrodes.[130–132] Ye and co-workers developed a facile hydrothermal carbonization process to effectively fabricate a 3D lignin/reduced graphene oxide (RGO) composite material (Fig. 6a).[133] The favorable SSA (1804 m^2 g^{-1}) and high electrical conductivity of the lignin–RGO electrode guarantee efficient electron and ion transport. An excellent rate capability with high capacitances of 190 F g^{-1} at 0.5 A g^{-1} and 133.9 F g^{-1} at 10 A g^{-1} in 6 M KOH were thus delivered. As per Fig. 6b, Jiang *et al.* synthesized lignin/RGO aerogels (LRGOs) by an activation-free strategy.[134] Graphene oxide was initially reduced by lignin and then spotlighted as a 3D template to modulate the

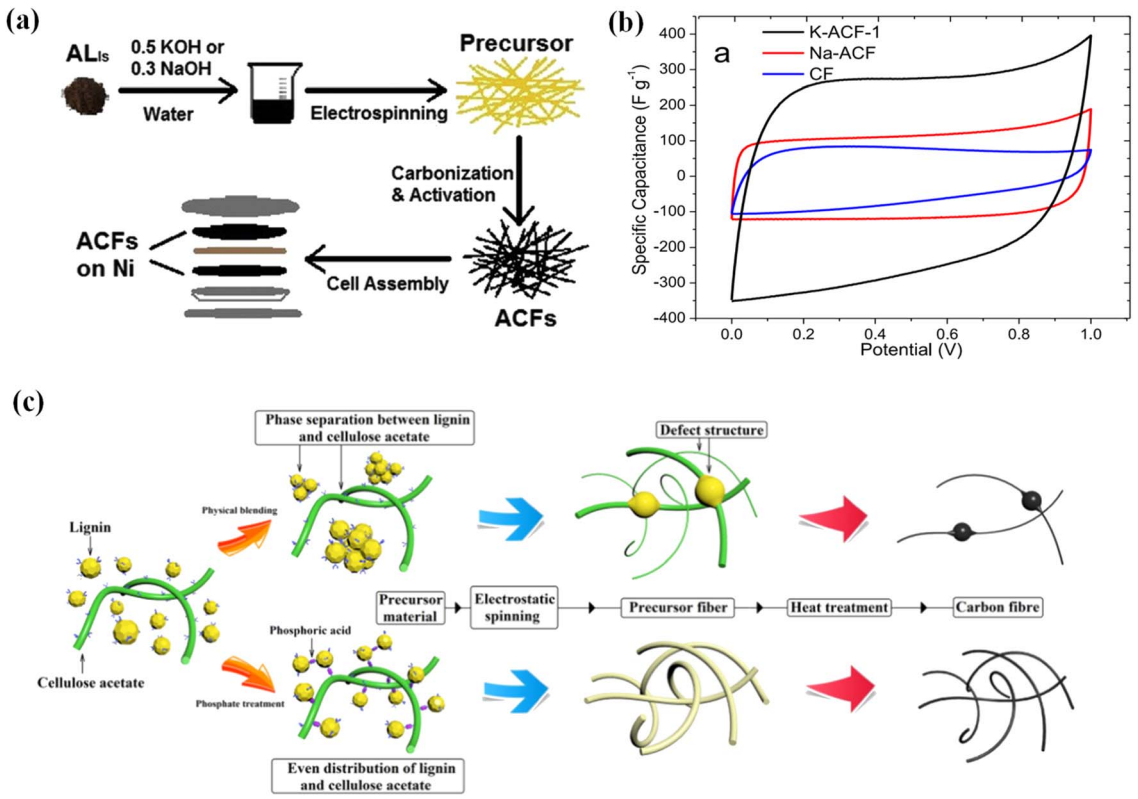

Fig. 5 (a) Schematic diagrams of the preparation of lignin-based porous submicron ACFs. (b) CV profiles of various ACFs. Adapted with permission from ref. 125. Copyright 2014 Elsevier. (c) Proposed mechanism of phosphoric acid-functionalized ACFs. Adapted with permission from ref. 126 Copyright 2020 American Chemical Society.

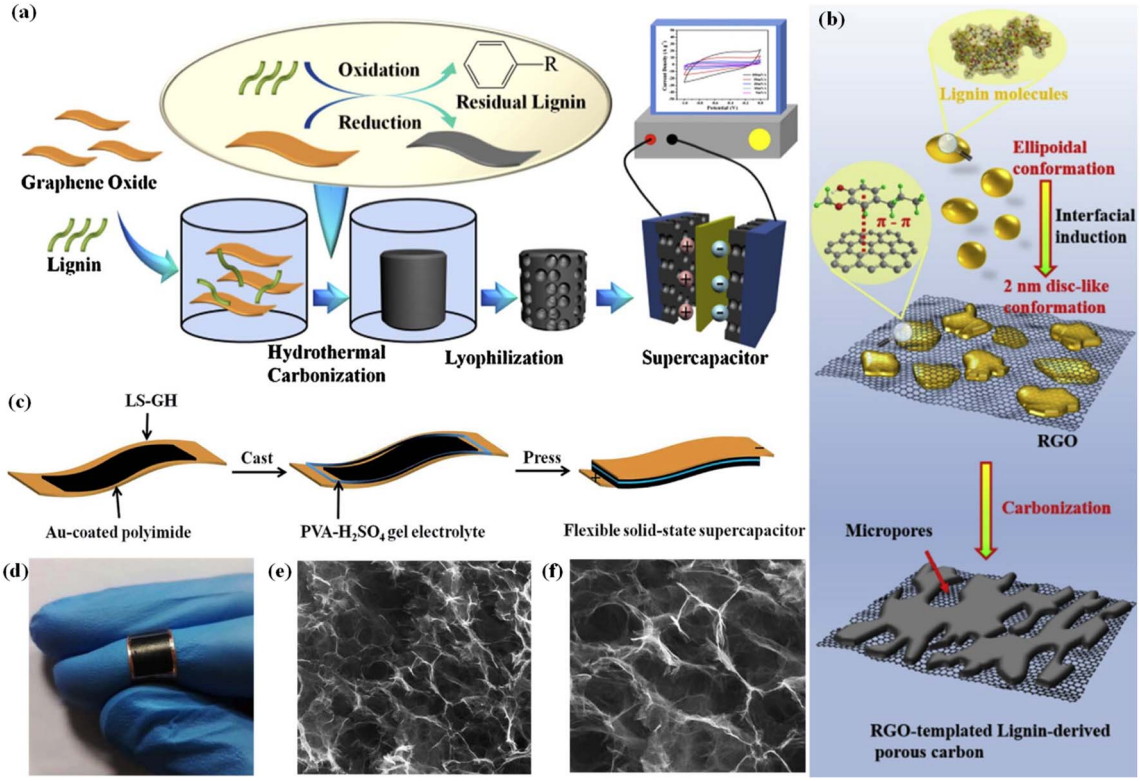

Fig. 6 (a) Schematic of the synthesis of the lignin–RGO composite. Adapted with permission from ref. 133. Copyright 2017 Elsevier. (b) A schematic diagram of the molecular conformation conversion of lignin and the preparation of micropores in RGO-templated pseudo-capacitors. Adapted with permission from ref. 134. Copyright 2020 Elsevier. (c) Illustration of the preparation of LS–GH flexible solid-state supercapacitors. (d) Digital photograph of the flexible device; SEM images of the interior microstructure at (e) low and (f) high magnification. Adapted with permission from ref. 135. Copyright 2017 Royal Society of Chemistry.

conformal conversion of lignin macromolecules from ellipsoidal to disk-shaped; finally, lignin was ordered on both sides of the RGO nanosheets. Further, through the carbonization process, LRGOs with favorable SSA and unique hierarchical porous architectures were obtained. In this fashion, the LRGOs electrode displayed a series of metrics including specific capacitance of 330 F g^{-1}, energy density of 11.3 W h kg^{-1} and power density of 2614 W kg^{-1} in 1 M H_2SO_4. It also showed an outstanding rate performance (>60%) and good cycle stability (100% after 10 000 cycles) in 1 M H_2SO_4. Li *et al.* manufactured a flexible metal-free supercapacitor by employing lignin-functionalized graphene hydrogel (Fig. 6c–f).[135] The integrated flexible solid-state supercapacitor device utilizing H_2SO_4–PVA gel as the electrolyte achieved a high specific capacitance (408 F g^{-1} at 1 A g^{-1}), outstanding cycle stability (84.4% after 10 000 cycles at 10 A g^{-1}), and a considerable energy density of 13.8 W h kg^{-1} at a power density of 500 W kg^{-1}, thanks to the reversible redox charge transfer of quinone groups in lignin.

3.2 Lignin-based electrodes for pseudo-capacitors

3.2.1 Metal oxide/lignin-derived carbon composite. Both metal oxides and conducting polymers can yield higher capacitances as compared with carbon materials, however, they encounter suboptimal cycle stability, high cost and process variability, which are not compatible with large-scale fabrication.[61] Thus, combining metal oxides or conducting polymers with lignin-based EDLCs to fabricate composite electrodes can result in them inheriting the advantages from the parents, thus achieving high-performance supercapacitors.[136–141] As an example, Ma and co-workers manufactured lignin-derived electrospun carbon nanofiber (ECNF) mats surface-decorated with MnO_2 nanowhiskers as binder-free supercapacitor electrodes.[142] The ECNF/MnO_2 mat electrodes display significantly enhanced electrochemical performance in comparison with the pure ECNF mat electrodes. Furthermore, the assembled symmetrical coin cell based on the optimal ECNF/MnO_2 mat can realize the superior gravimetric capacitance of 83.3 F g^{-1}, and a remarkable energy density of 84.3 W h kg^{-1} at the power density of 5.72 kW kg^{-1} in 1 M $LiPF_6$ electrolyte. Our group prepared the HPC/WO_3 composite *via* the carbonization and solvothermal process.[71] The composite can operate stably in the voltage window of −0.4 V to 1.0 V, and achieve the superior specific capacitance of 432 F g^{-1} at 0.5 A g^{-1} in 1 M H_2SO_4. The assembled asymmetric supercapacitor showed an energy density of 34.2 W h kg^{-1} at 14 300 W kg^{-1}. Additionally, the solid-state planar micro-supercapacitor device based on the HPC/WO_3 composite also exhibited a high areal specific capacitance of 20 mF cm^{-2} in the H_2SO_4–polyvinyl alcohol (PVA) gel electrolyte. Besides, our group further synthesized

$Ni_{4-x}Co_xWO_4$/HPC composite materials with various Co/Ni ratios *via* a facile co-precipitation method.[143] The optimal $Ni_3Co_1WO_4$/HPC electrode exhibited a specific capacitance of up to 1084 F g^{-1} at 0.5 A g^{-1} in 6 M KOH, along with an outstanding rate capability, due to the large SSA and strong synergistic effect between Co and Ni ions. The Faraday reactions are listed as follows:

$$Ni^{2+} + 3OH^- \leftrightarrow NiOOH + H_2O + e^- \quad (1)$$

$$Co^{2+} + 3OH^- \leftrightarrow CoOOH + H_2O + e^- \quad (2)$$

$$CoOOH + OH^- \leftrightarrow CoO_2 + H_2O + e^- \quad (3)$$

The assembled asymmetric supercapacitor can provide a wide voltage window of 1.6 V and give a superior energy density of 105.6 W h kg^{-1} at 400.5 W kg^{-1} in 6 M KOH, in conjunction with the considerable stability of 80.74% capacitance retention after 10 000 cycles. Moreover, Cao *et al.*[144] prepared the multi-channel carbon nanofiber (MCNFs)@SnO_2 nanocomposites *via* the co-electrospinning method, whereby poly(vinyl pyrrolidone)–$SnCl_2 \cdot 2H_2O$ and lignin–poly(methyl methacrylate) were used as the shell and core, respectively (Fig. 7a). Notably, the hollow structures function as fast electron transfer pathways to achieve intimate contact with electrolyte ions. Besides, $SnCl_2 \cdot 2H_2O$ not only serves as a pore-forming agent to enhance the SSA but also acts as a precursor for SnO_2 to provide pseudocapacitance for nanocomposites. Accordingly, the optimal nanocomposite electrode displays an excellent specific capacitance of 406 F g^{-1} at 0.5 A g^{-1} in 6 M KOH. Moreover, the specific capacitance can retain 95% after 10 000 cycles, indicative of exceptionable cycle stability.

In the past two decades, due to the considerable specific energy density, good electrochemical activity, nontoxicity, and environmental friendliness, ZnO has become one of the promising metal oxides for supercapacitors.[147–149] Fu *et al.* successfully constructed a lignin-derived carbon/ZnO (LDC/ZnO) composite with a 3D porous structure *via* electrostatic self-assembly. The composite was *in situ* carbonized by using ZnC_2O_4 particles as the catalyst and activator, leading to a large SSA and excellent conductivity (Fig. 7b).[145] The fabricated symmetric supercapacitor device based on LDC/ZnO electrodes achieved a capacitance of up to 193 F g^{-1} at 0.5 A g^{-1} using the PVA/KOH gel as the electrolyte, with considerable cycle stability. Furthermore, Ji and co-workers incorporated Ni and MnO_2 in lignin-based porous carbon materials (PC–Ni/MnO_2),[146] whereby $C_4H_6O_4Ni \cdot 4H_2O$ and $KMnO_4$ were utilized as a catalyst and a dopant, respectively. As illustrated in Fig. 7c, lignin is converted to highly graphitized carbon nanosheets and multi-layer graphene due to the catalytic effect of Ni during the carbonization process, while $KMnO_4$ decomposes into MnO_2 loading on the carbon material. As a result, the PC–Ni/MnO_2 can realize a superior gravimetric capacitance of 267.34 F g^{-1} at 0.1 A g^{-1} in 6 M KOH. Furthermore, the assembled symmetrical supercapacitor displays an energy density of 28 W h kg^{-1} and

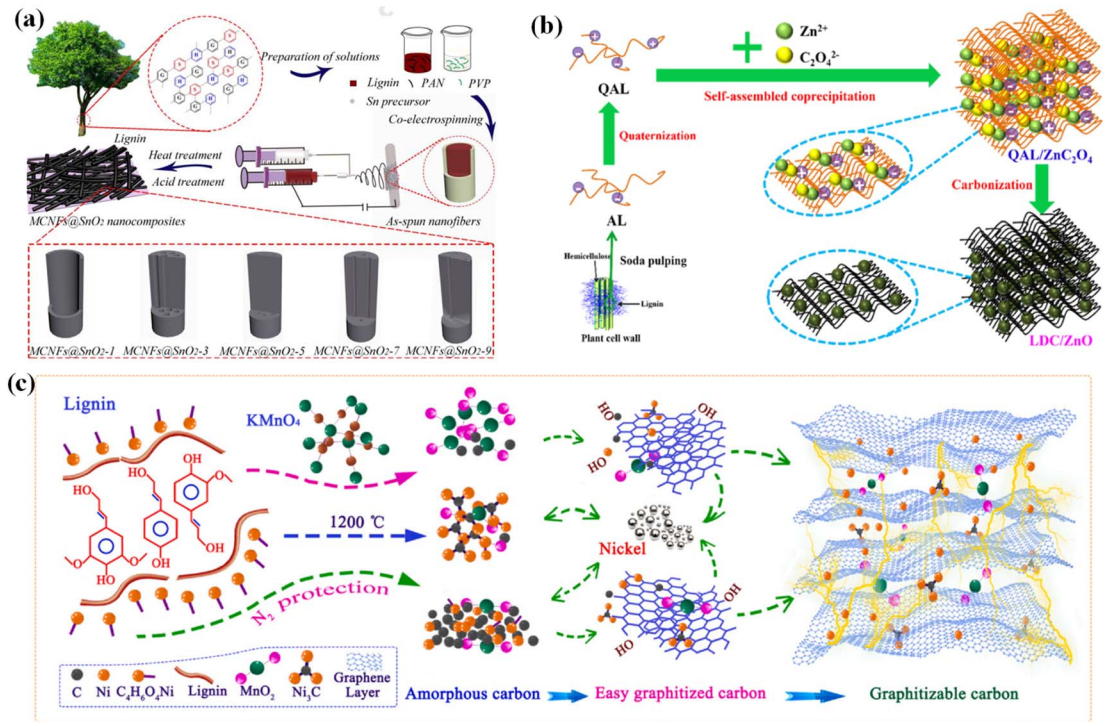

Fig. 7 (a) Schematic procedure for the preparation of MCNFs@SnO_2 nanocomposites. Adapted with permission from ref. 144. Copyright 2020 Elsevier. (b) Illustration of the fabrication mechanism of the LDC/ZnO materials. Reprinted with permission from ref. 145. Copyright 2019 American Chemical Society. (c) Proposed catalytic graphitization mechanism of Ni. Reprinted with permission from ref. 146. Copyright 2021 Elsevier.

a power density of 360 W kg^{-1}, with a favorable cycle stability after 5000 cycles in 6 M KOH.

3.2.2 Conductive polymer/lignin composites. Recent studies have shown that the abundant phenolic groups in lignin can form electroactive quinone–hydroquinone couples through a reversible redox reaction, enabling the development of high energy density electrode materials for supercapacitors.[150–154] Nonetheless, the insulating property of lignin hampers the utilization of these redox groups. Likewise, many efforts have been dedicated to combining lignin with conductive polymers to prepare composite electrodes with excellent electrochemical performance.[155] Milczarek *et al.* developed a series of composite materials based on the combination of polypyrrole (PPy) and lignosulfonate (LS) derivatives with redox functions (Fig. 8a).[86] It was suggested that interpenetrating networks of LS and PPy can be used for charge and energy storage. In particular, the quinone group in lignin can help to store the charges during redox cycling in an electroactive conjugated polymer/biopolymer composite. The redox processes are as follows with 0.1 M $HClO_4$ aqueous solution as the electrolyte:

$$PPy^0(Lig–QH_2) \rightarrow PPy^+(ClO_4^-)(Lig–QH_2) + e^- \quad (4)$$

$$PPy^+(ClO_4^-)(Lig–QH_2) \rightarrow PPy^+(ClO_4^-)(Lig–Q) + 2e^- + 2H^+ \quad (5)$$

Rojo *et al.* fabricated the full-cell supercapacitor device composed of lignin/PEDOT as the positive electrode and partially reduced graphite oxide (prGrO) as the negative electrode,[156] which delivered a higher capacitance of 34.6 F g^{-1} at 0.1 A g^{-1} in 0.1 M $HClO_4$ electrolyte in comparison with the symmetric cells of lignin/PEDOT and prGrO. The enhanced electrochemical properties of the asymmetric device can be ascribed to the synergistic effect between the homogeneous distribution of the pseudocapacitive centers and enhanced electrical conductivity triggered by the intimate combination of both materials in the same electrode. Ajjan *et al.* synthesized bio-composites *via* both oxidative chemical and electrochemical polymerization of poly(3,4-ethylenedioxythiophene) (PEDOT) by adopting lignin sulfonate as the dopant and surfactant.[157] Compared to reference PEDOT electrodes, the synthesized PEDOT/lignin composite electrodes exhibited an increased specific capacitance from 80.4 F g^{-1} to 170.4 F g^{-1} in a 0.1 M $HClO_4$/water : acetonitrile (9 : 1) mixed solvent, which is attributed to the additional pseudocapacitance of quinone moieties in lignin. In order to further improve the capacitance of the

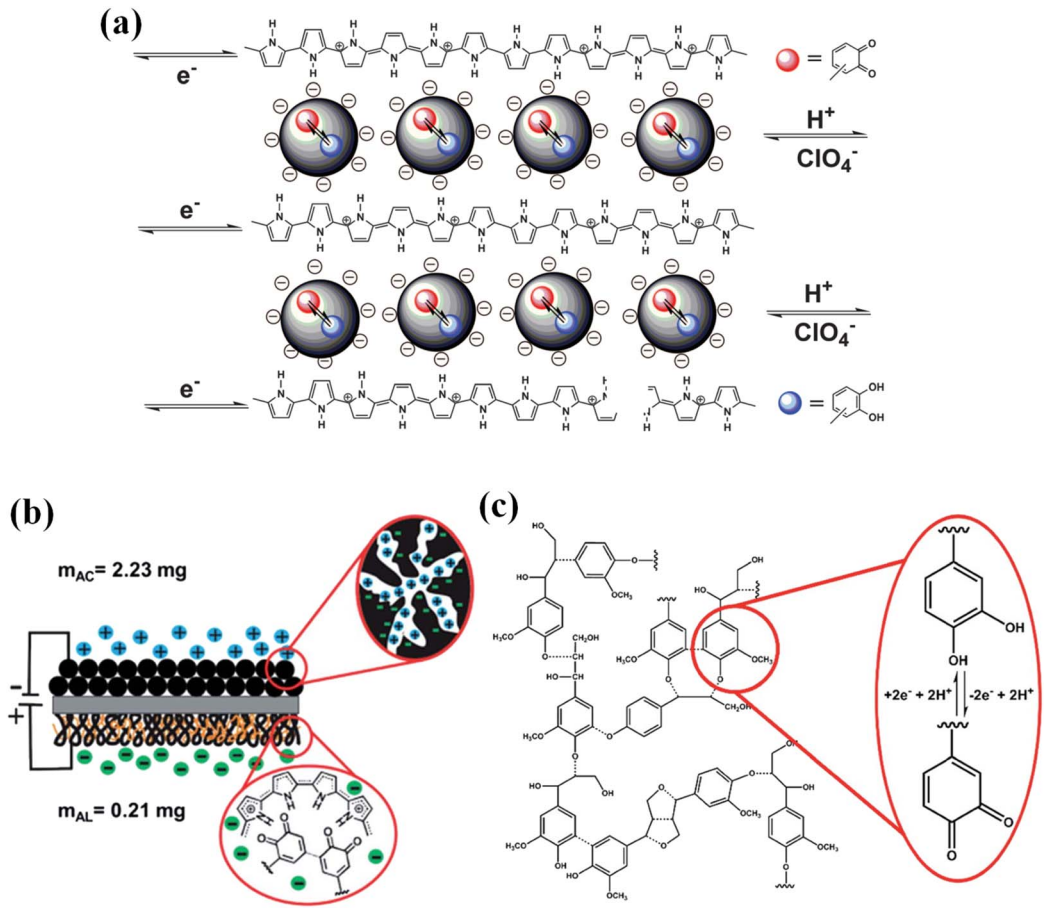

Fig. 8 (a) The electrochemical redox reaction of quinone functions in an LS biopolymer within a PPy matrix. Reprinted with permission from ref. 86. Copyright 2012 Science. (b) Schematic diagram of the PPy/AL–AC cell. (c) Illustrative schematic of the lignin structure along with the redox processes occurring between QH_2/Q. Adapted with permission from ref. 159. Copyright 2015 Royal Society of Chemistry.

composite electrode, they fabricated a trihybrid electrode (PEDOT/lignin/poly(aminoanthraquinone) (PAAQ)) by introducing a third component of PAAQ to provide more pseudocapacitance.[158] The trihybrid electrode manifested an excellent specific capacitance of 418 F g^{-1} at a current density of 1 A g^{-1} in 0.1 M $HClO_4$. The asymmetric supercapacitor device was assembled, wherein the PEDOT/lignin/PAAQ and PEDOT/PAAQ were employed as the positive and negative electrodes, respectively. Benefitting from the synergistic effect of the two electrodes, it demonstrated excellent electrochemical performance, allowing for a specific capacitance of 74 F g^{-1} in 0.1 M $HClO_4$. Additionally, a capacitance retention rate of 80% was identified after 10 000 cycles under a voltage window of 0.7 V. Alkali lignin (AL) accounts for 98% of lignin from paper-pulping; however, it encounters its own limitations due to its underdeveloped solubility in inorganic acids. To address this issue, Leguizamon *et al.* employed organic acid as the deposition solvent to fabricate PPy/AL electrodes (Fig. 8b).[159] The PPy/AL electrode delivers an improved capacitance of 444 F g^{-1} in 0.5 M H_2SO_4, which is 30% higher than the electrodes containing identical compositions of sodium lignosulfate and 56% higher than pure PPy electrodes. Fig. 8c shows the redox processes occurring between hydroquinone/quinone (QH_2/Q).

Despite these achievements, the cycle stability of the composite electrodes based on lignin with various conductive polymers is still restrained due to the instability of the conductive polymer during the electrochemical charging/discharging process. A ternary composite electrode comprised of phosphomolybdic acid (HMA, $H_3PMo_{12}O_{40}\cdot nH_2O$), lignin and PPy was fabricated by Admassie's group *via* one-step simultaneous electrochemical deposition.[160] The incorporation of HMA enabled the specific capacitance of the PPy–lignin composite to increase from 477 to 682 F g^{-1} at 1 A g^{-1} in 0.1 M $HClO_4$.

3.2.3 Heteroatom-doped pseudo-capacitor electrodes. Integrating heteroatoms (N, S, P, B and O) into the carbon matrix can create more opportunities for regulating the physical and chemical properties of electrodes, and simultaneously introduce reversible redox reactions, thus robustly promoting the capacitive performance of supercapacitors without compromising the rate and cycling performance.[161–168] Among the heteroatoms, N atoms are generally doped on the carbon skeleton to form stable active centers.[169] S doping can significantly improve the conductivity of carbon substrates due to the overlapping between the p-orbitals of sulfur atoms and sp^2-hybridized carbon atoms;[170] O doping can effectively improve the affinity and wettability of the material by the electrolyte.[171] With this in mind, Wang *et al.* fabricated N-doped pseudo-capacitors possessing a well-tailored porous structure and high SSA of 3130 m^2 g^{-1}.[172] Additionally, a specific capacitance of 273 F g^{-1} at 0.1 A g^{-1} in 6 M KOH electrolyte was obtained. Furthermore, the assembled all-solid supercapacitor device demonstrated a specific capacitance of 306 F g^{-1} at 0.1 A g^{-1} in KOH–PVA gel electrolyte. Based on this work, they further constructed the N-doped rod-shaped pseudo-capacitors derived from lignin.[173] Upon regulating the activation temperature, the pseudo-capacitors exhibited a high SSA with interconnected cavities, which provide more active sites to enhance the wettability between the electrode and electrolyte, thereby leading to the optimal specific capacitance of 336 F g^{-1} and a tiny resistance of 0.9 Ω in 6 M KOH. Chen and co-workers demonstrated that the addition of protein can prevent the beading of lignin due to its lower molecular weight and viscosity during electrospinning.[174] The synthesized N-doped protein/lignin fiber electrodes manifested a high capacitance of 410 F g^{-1} at 1 A g^{-1}, together with a considerable cycling performance in 6 M KOH. In another study, the N-doped HPC possessing a high SSA of 1867.4 m^2 g^{-1} and a favorable nitrogen-doped content of 3.6 at% was fabricated by Zhong's group, who used 1,6-hexanediamine as the crosslinking agent and nitrogen source.[163] Remarkably, the phenolic hydroxyl groups in lignin crosslinked with the amine groups in 1,6-hexanediamine, allowing for the formation of an exclusive 3D interconnected hierarchical porous architecture. The fabricated supercapacitor achieved a high specific capacitance of 370 F g^{-1} at 0.5 A g^{-1}. Moreover, after 3000 cycles, an excellent capacitance retention of 95.1% was obtained in 6 M KOH.

Co-doping with two or more kinds of heteroatoms is an efficient way to further boost the device performance through synergistic effects.[175–179] Tian *et al.* synthesized the nitrogen and sulfur co-doped 3D multilevel hierarchical porous carbons (N, S–HPCs) by utilizing sodium lignosulfonate as the C and S sources, while the polyaniline-coated polystyrene spheres were spotlighted as the N precursor and template for macropores (Fig. 9a).[164] Startlingly, this high N, S-doping content (up to 2.1 and 4.3 wt%) and lower internal series resistance boosted the specific capacitance of the N, S–HPC electrode material to 269 F g^{-1} (at 0.5 A g^{-1}) from 16.9 F g^{-1} of solely carbonized lignin in 6 M KOH (Fig. 9b and c). As depicted in Fig. 9d, this N–S–HPC electrode also demonstrated outstanding rate performance (62% capacitance retention at 50 A g^{-1}) and cycle stability (98.4% capacitance retention after 10 000 cycles) in 6 M KOH. Moreover, Liu *et al.* fabricated the O–N–S co-doped HPCs with a large SSA (338–1307 m^2 g^{-1}) by directly pyrolyzing kraft lignin.[180] As expected, the fabricated symmetric supercapacitor in aqueous electrolyte delivered a high energy density of 66.8 W h kg^{-1} at a power density of 1.75 kW kg^{-1} while utilizing $EMIMBF_4$ as the electrolyte. Our group successfully synthesized O, N and S co-doped HPC *via* a carbonization activation route using enzymatically hydrolyzed lignin as the carbon source.[181] The obtained HPC has large SSA, abundant multiscale pores and high O, N, and S doping density. The faradaic redox reactions of N–O–S-containing functional groups in KOH electrolyte are shown in the following equations:[182–186]

$$\text{–C–N–C–} + H_2O + e^- \leftrightarrow \text{–C–NH–C–} + OH^- \quad (6)$$

$$\text{–C–S–C–} + H_2O + 3e^- \leftrightarrow \text{–C–}SO_2\text{–C–} + 3OH^- \quad (7)$$

$$\text{–C=O} + H_2O + 2e^- \leftrightarrow \text{–CH–}O^- + OH^- \quad (8)$$

Consequently, the HPC electrode delivered a superior specific capacitance of 318 F g^{-1} at 0.5 A g^{-1} and excellent rate

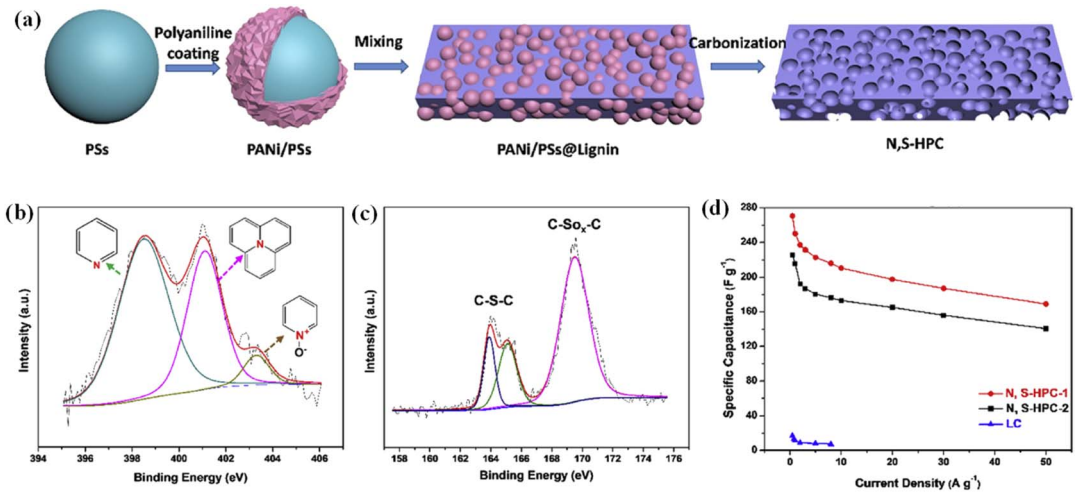

Fig. 9 (a) Schematic preparation procedure for N, S–HPC. High-resolution N1s (b), S2p (c) XPS of N, S–HPC-1. (d) The specific capacitances of the samples at various current densities. Adapted with permission from ref. 164. Copyright 2019 Elsevier.

performance (62% retention at 50 A g^{-1}) in 6 M KOH. The assembled asymmetric supercapacitor yielded a high energy density of 16.7 W h kg^{-1} at a power density of 249 W kg^{-1} and outstanding cycle stability (99.58% retention over 10 000 cycles) in 6 M KOH.

3.3 Applications of lignin-based supercapacitors

Owing to their excellent flexibility, fast charging and discharging capabilities, and durable service lifetime, flexible supercapacitors (FSCs) have successfully attracted broad research interest with an increasing demand for flexible and wearable electronics.[9,187,188] Commonly used electrode materials for FSCs can be categorized into carbon materials (*i.e.*, ACs, CNTs, and graphene), transition metal oxides/hydroxides, and conductive polymers.[189–193] Among them, graphene and CNTs are suitable for preparing FSCs due to their high SSA, excellent conductivity and mechanical properties. Nevertheless, when they are utilized to prepare large-area electrodes, the SSA and capacitance performance will be compromised significantly due to undesirable agglomeration.

Thanks to the unique structural characteristics, lignin can interact with graphene and CNTs through π–π effects to offset this irreversible agglomeration, having exhibited a huge potential for FSCs.[194,195] Peng *et al.* fabricated FSCs by utilizing a lignosulfonate/single-walled CNT composite as the electrode and cellulose/Li_2SO_4 hydrogel as the electrolyte, which delivered an outstanding specific capacitance of 292 F g^{-1} at 0.5 A g^{-1} coupled with excellent rate capability, and a high energy density of 17.1 W h kg^{-1} at the power density of 324 W kg^{-1}.[196] The FSCs also exhibited excellent mechanical stability, retaining 98% of the initial capacitance after 1000 bending cycles. This excellent performance can be attributed to the synergistic effect of lignosulfonate-based carbon and CNT, as well as the superior 3D porous network structure. Moreover, Jha *et al.* assembled FSCs composed of Al/AC/lig–MnO_2 as the anode, Al/AC as the cathode, and (PVA)/H_3PO_4 gel as the electrolyte.[197] Due to their synergistic effect, the FSCs yielded a high specific capacitance of 5.52 mF cm^{-2}, excellent mechanical stability (97.5% retention after 2000 cycles), and a favorable energy density of 14.11 W h kg^{-1} at the power density of 1 kW kg^{-1}.

In the quest for renewable and highly efficient energy storage devices, Park *et al.* prepared all-lignin-based FSCs based on lignin hydrogel electrolytes and electrospun lignin/PAN nanofiber electrodes.[18] The lignin hydrogel electrolytes display high ionic conductivity and excellent mechanical integrity, and the lignin-based carbon/PAN composite electrode possessing interconnected porous channels exhibits exceptional charge storage capability and kinetics. The FSCs attained a high capacitance of 129.23 F g^{-1} and beneficial capacitance retention of 95% over 10 000 cycles, as well as excellent flexibility and durability under diverse bending angles. Moreover, a maximum energy density of 4.49 W h kg^{-1} at the power density of 2.63 kW kg^{-1} was achieved. Accordingly, utilizing renewable lignin-based materials to assemble environmentally friendly and biocompatible FSCs provides a novel option for the development of sustainable energy storage systems.

4. Conclusion and prospectives

This review has comprehensively summarized the recent developments in the design and fabrication of lignin-based electrode materials for supercapacitors. It has been validated that lignin can be utilized as precursors to fabricate efficient PCs (*e.g.* ACs, templated carbon and CFs), which are prospective electrode materials for supercapacitors. Nevertheless, despite the progress to date, the study of lignin-based electrode materials is still in its infancy, and there are still some prospects that are worthy of attention in the future.

(1) The physicochemical properties of lignin (*e.g.*, molecular weight, solubility, and purity) depending on the natural sources and extraction methods will play a decisive role in the properties of the derivative carbon materials. Thus, further endeavors should be devoted to developing feasible methods to attain

stable and homogeneous lignin, in favor of optimizing the properties of carbon materials for specific applications.

(2) The carbon materials converted from lignin generally possess controllable microstructures and diverse morphologies. However, the current converting strategies are complex and costly, which severely limits their large-scale applications. Of special note, the commonly utilized alkali activators are highly corrosive to the equipment and effortlessly lead to environmental pollution. Therefore, future research should focus on developing a green route for the large-scale production of lignin carbon materials.

(3) The structure–function relationship between the microstructure of lignin-based carbons and their charge storage performance/mechanisms remains ambiguous. Operando characterization techniques, such as ATR-FTIR, EQCM-D and *in situ* NMR, *etc.*, are highly desirable to investigate the alteration of surface states of lignin-based PCs during the electrochemical process, which is beneficial to expound the energy storage mechanism and lay a foundation for designing and optimizing lignin-based energy storage materials.

Conflicts of interest

The authors declare that they have no known competing financial interests or personal relationships that could have appeared to influence the work reported in this paper.

Acknowledgements

This research is financially supported by the National Natural Science Foundation of China (21908013, U20A20252, 22279140), the innovation fund project of Dalian Institute of Chemical Physics (DICP I202025), the Cooperation Foundation of Dalian National Laboratory for Clean Energy of the Chinese Academy of Sciences (DNL202015), Natural Science Foundation of Liaoning Province of China (2021-MS-016), Research Project of Education Department of Liaoning Province (LJKQZ2021115), Dalian Young Star of Science and Technology Project (2021RQ020, 2021RQ121).

References

1 N. Chang, T. Li, R. Li, S. Wang, Y. Yin, H. Zhang and X. Li, *Energy Environ. Sci.*, 2020, **13**, 3527–3535.
2 T. Xu, H. Du, H. Liu, W. Liu, X. Zhang, C. Si, P. Liu and K. Zhang, *Adv. Mater.*, 2021, **33**, 2101368.
3 S. Chen, L. Qiu and H.-M. Cheng, *Chem. Rev.*, 2020, **120**, 2811–2878.
4 J. Xiao, J. Han, C. Zhang, G. Ling, F. Kang and Q.-H. Yang, *Adv. Energy Mater.*, 2022, **12**, 2100775.
5 H. Li, Z. Tang, Z. Liu and C. Zhi, *Joule*, 2019, **3**, 613–619.
6 W. Guo, C. Yu, S. Li and J. Qiu, *Energy Environ. Sci.*, 2021, **14**, 576–601.
7 M. Salanne, B. Rotenberg, K. Naoi, K. Kaneko, P. L. Taberna, C. P. Grey, B. Dunn and P. Simon, *Nat. Energy*, 2016, **1**, 16070.
8 W. Zuo, R. Li, C. Zhou, Y. Li, J. Xia and J. Liu, *Adv. Sci.*, 2017, **4**, 1600539.
9 Y. Wang, X. Wu, Y. Han and T. Li, *J. Energy Storage*, 2021, **42**, 103053.
10 J. Chmiola, C. Largeot, P.-L. Taberna, P. Simon and Y. Gogotsi, *Science*, 2010, **328**, 480–483.
11 X. Jin, L. Song, H. Yang, C. Dai, Y. Xiao, X. Zhang, Y. Han, C. Bai, B. Lu, Q. Liu, Y. Zhao, J. Zhang, Z. Zhang and L. Qu, *Energy Environ. Sci.*, 2021, **14**, 3075–3085.
12 S. Kumar, G. Saeed, L. Zhu, K. N. Hui, N. H. Kim and J. H. Lee, *Chem. Eng. J.*, 2021, **403**, 126352.
13 W. Raza, F. Ali, N. Raza, Y. Luo, K.-H. Kim, J. Yang, S. Kumar, A. Mehmood and E. E. Kwon, *Nano Energy*, 2018, **52**, 441–473.
14 L. Fan, K. Lin, J. Wang, R. Ma and B. Lu, *Adv. Mater.*, 2018, **30**, 1800804.
15 P. Divya and R. Rajalakshmi, *J. Energy Storage*, 2020, **27**, 101149.
16 H. H. Rana, J. H. Park, G. S. Gund and H. S. Park, *Energy Storage Mater.*, 2020, **25**, 70–75.
17 D. Zhao, C. Chen, Q. Zhang, W. Chen, S. Liu, Q. Wang, Y. Liu, J. Li and H. Yu, *Adv. Energy Mater.*, 2017, **7**, 1700739.
18 J. H. Park, H. H. Rana, J. Y. Lee and H. S. Park, *J. Mater. Chem. A*, 2019, **7**, 16962–16968.
19 C. G. Yoo, X. Meng, Y. Pu and A. J. Ragauskas, *Bioresour. Technol.*, 2020, **301**, 122784.
20 J. Ralph, C. Lapierre and W. Boerjan, *Curr. Opin. Biotechnol.*, 2019, **56**, 240–249.
21 C. Chio, M. Sain and W. Qin, *Renewable Sustainable Energy Rev.*, 2019, **107**, 232–249.
22 D. S. Bajwa, G. Pourhashem, A. H. Ullah and S. G. Bajwa, *Ind. Crops Prod.*, 2019, **139**, 111526.
23 K. Liu, H. Du, T. Zheng, W. Liu, M. Zhang, H. Liu, X. Zhang and C. Si, *Green Chem.*, 2021, **23**, 9723–9746.
24 H. Wang, F. Fu, M. Huang, Y. Feng, D. Han, Y. Xi, W. Xiong, D. Yang and L. Niu, *Nano Mater. Sci.*, 2022, DOI: **10.1016/j.nanoms.2022.01.002**.
25 L. T. Nguyen, D.-P. Phan, A. Sarwar, M. H. Tran, O. K. Lee and E. Y. Lee, *Ind. Crops Prod.*, 2021, **161**, 113219.
26 R. Radhakrishnan, P. Patra, M. Das and A. Ghosh, *Renewable Sustainable Energy Rev.*, 2021, **149**, 111368.
27 J. Ni, Y.-T. Wu, F. Tao, Y. Peng and P. Xu, *J. Am. Chem. Soc.*, 2018, **140**, 16001–16005.
28 M. Chen, F. Malaret, A. E. J. Firth, P. Verdía, A. R. Abouelela, Y. Chen and J. P. Hallett, *Green Chem.*, 2020, **22**, 5161–5178.
29 S. Hu and Y.-L. Hsieh, *Int. J. Biol. Macromol.*, 2016, **82**, 856–862.
30 B. M. Cerrutti, C. S. de Souza, A. Castellan, R. Ruggiero and E. Frollini, *Ind. Crops Prod.*, 2012, **36**, 108–115.
31 C. Cai, Y. Bao, X. Zhan, X. Lin, H. Lou, Y. Pang, Y. Qian and X. Qiu, *Green Chem.*, 2019, **21**, 1141–1151.
32 J.-H. Choi, S.-K. Jang, J.-H. Kim, S.-Y. Park, J.-C. Kim, H. Jeong, H.-Y. Kim and I.-G. Choi, *Renewable Energy*, 2019, **130**, 952–960.
33 M. Parit and Z. Jiang, *Int. J. Biol. Macromol.*, 2020, **165**, 3180–3197.

34 B. M. Upton and A. M. Kasko, *Chem. Rev.*, 2016, **116**, 2275–2306.
35 W. Pei, W. Shang, C. Liang, X. Jiang, C. Huang and Q. Yong, *Ind. Crops Prod.*, 2020, **154**, 112638.
36 D. Kai, M. J. Tan, P. L. Chee, Y. K. Chua, Y. L. Yap and X. J. Loh, *Green Chem.*, 2016, **18**, 1175–1200.
37 M. Luo, H. Lin, B. Li, Y. Dong, Y. He and L. Wang, *Bioresour. Technol.*, 2018, **259**, 312–318.
38 I. P. Pérez, A. M. Rodríguez Pasandín, J. C. Pais and P. A. Alves Pereira, *J. Cleaner Prod.*, 2019, **220**, 87–98.
39 C. Xiong, M. Li, S. Nie, W. Dang, W. Zhao, L. Dai and Y. Ni, *J. Power Sources*, 2020, **471**, 228448.
40 W. Zhang, J. Yin, C. Wang, L. Zhao, W. Jian, K. Lu, H. Lin, X. Qiu and H. N. Alshareef, *Small Methods*, 2021, **5**, 2100896.
41 J. Zhu, C. Yan, X. Zhang, C. Yang, M. Jiang and X. Zhang, *Prog. Energy Combust. Sci.*, 2020, **76**, 100788.
42 S. Guo, H. Li, X. Zhang, H. Nawaz, S. Chen, X. Zhang and F. Xu, *Carbon*, 2021, **174**, 500–508.
43 W. Schutyser, T. Renders, S. Van den Bosch, S. F. Koelewijn, G. T. Beckham and B. F. Sels, *Chem. Soc. Rev.*, 2018, **47**, 852–908.
44 R. Liu, L. Dai, C. Xu, K. Wang, C. Zheng and C. Si, *ChemSusChem*, 2020, **13**, 4266–4283.
45 W. Lin, S. Xing, Y. Jin, X. Lu, C. Huang and Q. Yong, *Bioresour. Technol.*, 2020, **306**, 123163.
46 L. Zheng, P. Yu, Y. Zhang, P. Wang, W. Yan, B. Guo, C. Huang and Q. Jiang, *Int. J. Biol. Macromol.*, 2021, **176**, 13–25.
47 L. Dai, M. Ma, J. Xu, C. Si, X. Wang, Z. Liu and Y. Ni, *Chem. Mater.*, 2020, **32**, 4324–4330.
48 A. Naseem, S. Tabasum, K. M. Zia, M. Zuber, M. Ali and A. Noreen, *Int. J. Biol. Macromol.*, 2016, **93**, 296–313.
49 S. Gharehkhani, Y. Zhang and P. Fatehi, *Prog. Energy Combust. Sci.*, 2019, **72**, 59–89.
50 H. Wang, Y. Pu, A. Ragauskas and B. Yang, *Bioresour. Technol.*, 2019, **271**, 449–461.
51 H. Liu, T. Xu, K. Liu, M. Zhang, W. Liu, H. Li, H. Du and C. Si, *Ind. Crops Prod.*, 2021, **165**, 113425.
52 A. K. Mondal, D. Xu, S. Wu, Q. Zou, W. Lin, F. Huang and Y. Ni, *Int. J. Biol. Macromol.*, 2022, **207**, 48–61.
53 W.-J. Liu, H. Jiang and H.-Q. Yu, *Green Chem.*, 2015, **17**, 4888–4907.
54 W. Fang, S. Yang, X.-L. Wang, T.-Q. Yuan and R.-C. Sun, *Green Chem.*, 2017, **19**, 1794–1827.
55 M. Norgren and H. Edlund, *Curr. Opin. Colloid Interface Sci.*, 2014, **19**, 409–416.
56 D. Gan, W. Xing, L. Jiang, J. Fang, C. Zhao, F. Ren, L. Fang, K. Wang and X. Lu, *Nat. Commun.*, 2019, **10**, 1487.
57 P. Figueiredo, K. Lintinen, J. T. Hirvonen, M. A. Kostiainen and H. A. Santos, *Prog. Mater. Sci.*, 2018, **93**, 233–269.
58 V. K. Ponnusamy, D. D. Nguyen, J. Dharmaraja, S. Shobana, J. R. Banu, R. G. Saratale, S. W. Chang and G. Kumar, *Bioresour. Technol.*, 2019, **271**, 462–472.
59 J. Xu, C. Li, L. Dai, C. Xu, Y. Zhong, F. Yu and C. Si, *ChemSusChem*, 2020, **13**, 4284–4295.
60 N. Kamimura, S. Sakamoto, N. Mitsuda, E. Masai and S. Kajita, *Curr. Opin. Biotechnol.*, 2019, **56**, 179–186.
61 J. L. Espinoza-Acosta, P. I. Torres-Chávez, J. L. Olmedo-Martínez, A. Vega-Rios, S. Flores-Gallardo and E. A. Zaragoza-Contreras, *J. Energy Chem.*, 2018, **27**, 1422–1438.
62 J. Mei, X. Shen, L. Gang, H. Xu, F. Wu and L. Sheng, *Bioresour. Technol.*, 2020, **310**, 123445.
63 C. Crestini, H. Lange, M. Sette and D. S. Argyropoulos, *Green Chem.*, 2017, **19**, 4104–4121.
64 G. Gellerstedt, *Ind. Crops Prod.*, 2015, **77**, 845–854.
65 S. Sen, S. Patil and D. S. Argyropoulos, *Green Chem.*, 2015, **17**, 4862–4887.
66 R. Deshpande, L. Sundvall, H. Grundberg, G. Henriksson and M. Lawoko, *Ind. Crops Prod.*, 2022, **177**, 114391.
67 N.-E. E. Mansouri and J. Salvadó, *Ind. Crops Prod.*, 2006, **24**, 8–16.
68 M. N. Collins, M. Nechifor, F. Tanasă, M. Zănoagă, A. McLoughlin, M. A. Stróżyk, M. Culebras and C.-A. Teacă, *Int. J. Biol. Macromol.*, 2019, **131**, 828–849.
69 A. G. Vishtal and A. Kraslawski, *Bioresources*, 2011, **6**, 22.
70 H. Li, F. Shi, Q. An, S. Zhai, K. Wang and Y. Tong, *Int. J. Biol. Macromol.*, 2021, **166**, 923–933.
71 F. Shi, J. Li, J. Xiao, X. Zhao, H. Li, Q. An, S. Zhai, K. Wang, L. Wei and Y. Tong, *Int. J. Biol. Macromol.*, 2021, **190**, 11–18.
72 L. L. Zhang and X. S. Zhao, *Chem. Soc. Rev.*, 2009, **38**, 2520–2531.
73 S. S. Mofarah, E. Adabifiroozjaei, Y. Yao, P. Koshy, S. Lim, R. Webster, X. Liu, R. Khayyam Nekouei, C. Cazorla, Z. Liu, Y. Wang, N. Lambropoulos and C. C. Sorrell, *Nat. Commun.*, 2019, **10**, 2594.
74 A. Muzaffar, M. B. Ahamed, K. Deshmukh and J. Thirumalai, *Renewable Sustainable Energy Rev.*, 2019, **101**, 123–145.
75 Y. Wang, Y. Song and Y. Xia, *Chem. Soc. Rev.*, 2016, **45**, 5925–5950.
76 E. Lim, C. Jo and J. Lee, *Nanoscale*, 2016, **8**, 7827–7833.
77 D. Sheberla, J. C. Bachman, J. S. Elias, C.-J. Sun, Y. Shao-Horn and M. Dincă, *Nat. Mater.*, 2017, **16**, 220–224.
78 G. Zhao, C. Chen, D. Yu, L. Sun, C. Yang, H. Zhang, Y. Sun, F. Besenbacher and M. Yu, *Nano Energy*, 2018, **47**, 547–555.
79 M. Sevilla and R. Mokaya, *Energy Environ. Sci.*, 2014, **7**, 1250–1280.
80 R. Rao, C. L. Pint, A. E. Islam, R. S. Weatherup, S. Hofmann, E. R. Meshot, F. Wu, C. Zhou, N. Dee, P. B. Amama, J. Carpena-Nuñez, W. Shi, D. L. Plata, E. S. Penev, B. I. Yakobson, P. B. Balbuena, C. Bichara, D. N. Futaba, S. Noda, H. Shin, K. S. Kim, B. Simard, F. Mirri, M. Pasquali, F. Fornasiero, E. I. Kauppinen, M. Arnold, B. A. Cola, P. Nikolaev, S. Arepalli, H.-M. Cheng, D. N. Zakharov, E. A. Stach, J. Zhang, F. Wei, M. Terrones, D. B. Geohegan, B. Maruyama, S. Maruyama, Y. Li, W. W. Adams and A. J. Hart, *ACS Nano*, 2018, **12**, 11756–11784.
81 J.-H. Lee and S.-J. Park, *Carbon*, 2020, **163**, 1–18.
82 H. Li, J. Liang, H. Li, X. Zheng, Y. Tao, Z.-H. Huang and Q.-H. Yang, *J. Energy Chem.*, 2019, **31**, 95–100.
83 M. F. El-Kady, Y. Shao and R. B. Kaner, *Nat. Rev. Mater.*, 2016, **1**, 16033.

84 Y. Zhu, S. Murali, M. D. Stoller, K. J. Ganesh, W. Cai, P. J. Ferreira, A. Pirkle, R. M. Wallace, K. A. Cychosz, M. Thommes, D. Su, E. A. Stach and R. S. Ruoff, *Science*, 2011, **332**, 1537–1541.
85 M. Boota and Y. Gogotsi, *Adv. Energy Mater.*, 2019, **9**, 1802917.
86 G. Milczarek and O. Inganäs, *Science*, 2012, **335**, 1468–1471.
87 A. Ehsani, M. K. Moftakhar and F. karimi, *J. Energy Storage*, 2021, **35**, 102291.
88 Z. Liao, Y.-H. Zhu, G.-T. Sun, L. Qiu and M.-Q. Zhu, *Ind. Crops Prod.*, 2022, **175**, 114266.
89 M. L. Aparna, G. R. Rao and T. Thomas, *J. Energy Storage*, 2022, **48**, 104048.
90 B. Li, F. Dai, Q. Xiao, L. Yang, J. Shen, C. Zhang and M. Cai, *Energy Environ. Sci.*, 2016, **9**, 102–106.
91 M. Klose, R. Reinhold, F. Logsch, F. Wolke, J. Linnemann, U. Stoeck, S. Oswald, M. Uhlemann, J. Balach, J. Markowski, P. Ay and L. Giebeler, *ACS Sustainable Chem. Eng.*, 2017, **5**, 4094–4102.
92 Y. Wu, J.-P. Cao, X.-Y. Zhao, Q.-Q. Zhuang, Z. Zhou, Y. Huang and X.-Y. Wei, *Appl. Surf. Sci.*, 2020, **508**, 144536.
93 Y. Xi, D. Yang, X. Qiu, H. Wang, J. Huang and Q. Li, *Ind. Crops Prod.*, 2018, **124**, 747–754.
94 S. Li, K. Han, J. Li, M. Li and C. Lu, *Microporous Mesoporous Mater.*, 2017, **243**, 291–300.
95 B. Szczęśniak, J. Phuriragpitikhon, J. Choma and M. Jaroniec, *J. Mater. Chem. A*, 2020, **8**, 18464–18491.
96 W. Jian, W. Zhang, B. Wu, X. Wei, W. Liang, X. Zhang, F. Wen, L. Zhao, J. Yin, K. Lu and X. Qiu, *ACS Appl. Mater. Interfaces*, 2022, **14**, 5425–5438.
97 W. Zhang, M. Zhao, R. Liu, X. Wang and H. Lin, *Colloids Surf., A*, 2015, **484**, 518–527.
98 Y. Wu, J.-P. Cao, Z.-Q. Hao, X.-Y. Zhao, Q.-Q. Zhuang, J.-S. Zhu, X.-Y. Wang and X.-Y. Wei, *Int. J. Electrochem. Sci.*, 2017, **12**, 7227–7239.
99 C. Chen, D. Yu, G. Zhao, B. Du, W. Tang, L. Sun, Y. Sun, F. Besenbacher and M. Yu, *Nano Energy*, 2016, **27**, 377–389.
100 B. Chang, Y. Guo, Y. Li, H. Yin, S. Zhang, B. Yang and X. Dong, *J. Mater. Chem. A*, 2015, **3**, 9565–9577.
101 L. Qie, W. Chen, H. Xu, X. Xiong, Y. Jiang, F. Zou, X. Hu, Y. Xin, Z. Zhang and Y. Huang, *Energy Environ. Sci.*, 2013, **6**, 2497–2504.
102 A. B. Fuertes and M. Sevilla, *ACS Appl. Mater. Interfaces*, 2015, **7**, 4344–4353.
103 N. Guo, M. Li, X. Sun, F. Wang and R. Yang, *Green Chem.*, 2017, **19**, 2595–2602.
104 K. Zhang, M. Liu, T. Zhang, X. Min, Z. Wang, L. Chai and Y. Shi, *J. Mater. Chem. A*, 2019, **7**, 26838–26848.
105 F. Fu, D. Yang, W. Zhang, H. Wang and X. Qiu, *Chem. Eng. J.*, 2020, **392**, 123721.
106 R. Ruiz-Rosas, M. J. Valero-Romero, D. Salinas-Torres, J. Rodríguez-Mirasol, T. Cordero, E. Morallón and D. Cazorla-Amorós, *ChemSusChem*, 2014, **7**, 1458–1467.
107 D. Saha, Y. Li, Z. Bi, J. Chen, J. K. Keum, D. K. Hensley, H. A. Grappe, H. M. Meyer, S. Dai, M. P. Paranthaman and A. K. Naskar, *Langmuir*, 2014, **30**, 900–910.
108 S. Herou, M. C. Ribadeneyra, R. Madhu, V. Araullo-Peters, A. Jensen, P. Schlee and M. Titirici, *Green Chem.*, 2019, **21**, 550–559.
109 H. Li, D. Yuan, C. Tang, S. Wang, J. Sun, Z. Li, T. Tang, F. Wang, H. Gong and C. He, *Carbon*, 2016, **100**, 151–157.
110 Y. Zhang, B. Yu, J. Zhang, X. Ding, J. Zeng, M. Chen and C. Wang, *ChemElectroChem*, 2018, **5**, 2142–2149.
111 Y. Song, J. Liu, K. Sun and W. Xu, *RSC Adv.*, 2017, **7**, 48324–48332.
112 B. Du, H. Zhu, L. Chai, J. Cheng, X. Wang, X. Chen, J. Zhou and R.-C. Sun, *Ind. Crops Prod.*, 2021, **170**, 113745.
113 M. B. Poudel and H. J. Kim, *Chem. Eng. J.*, 2022, **429**, 132345.
114 H. Wang, H. Niu, H. Wang, W. Wang, X. Jin, H. Wang, H. Zhou and T. Lin, *J. Power Sources*, 2021, **482**, 228986.
115 P. Schlee, O. Hosseinaei, C. A. O' Keefe, M. J. Mostazo-López, D. Cazorla-Amorós, S. Herou, P. Tomani, C. P. Grey and M.-M. Titirici, *J. Mater. Chem. A*, 2020, **8**, 23543–23554.
116 S. Hérou, J. J. Bailey, M. Kok, P. Schlee, R. Jervis, D. J. L. Brett, P. R. Shearing, M. C. Ribadeneyra and M. Titirici, *Adv. Sci.*, 2021, **8**, 2100016.
117 W. Qu, P. Hu, J. Liu, H. Jin and K. Wang, *J. Cleaner Prod.*, 2022, **343**, 131030.
118 M. Zhu, H. Liu, Q. Cao, H. Zheng, D. Xu, H. Guo, S. Wang, Y. Li and J. Zhou, *ACS Sustainable Chem. Eng.*, 2020, **8**, 12831–12841.
119 T. Mukhiya, B. Dahal, G. P. Ojha, D. Kang, T. Kim, S.-H. Chae, A. Muthurasu and H. Y. Kim, *Chem. Eng. J.*, 2019, **361**, 1225–1234.
120 E. Svinterikos, I. Zuburtikudis and M. Al-Marzouqi, *ACS Sustainable Chem. Eng.*, 2020, **8**, 13868–13893.
121 U. Kurtan, H. Aydın, B. Büyük, U. Şahintürk, M. A. Almessiere and A. Baykal, *J. Energy Storage*, 2020, **32**, 101671.
122 P. Schlee, S. Herou, R. Jervis, P. R. Shearing, D. J. L. Brett, D. Baker, O. Hosseinaei, P. Tomani, M. M. Murshed, Y. Li, M. J. Mostazo-Lopez, D. Cazorla-Amoros, A. B. Jorge Sobrido and M. M. Titirici, *Chem. Sci.*, 2019, **10**, 2980–2988.
123 M. Zhou, A. Bahi, Y. Zhao, L. Lin, F. Ko, P. Servati, S. Soltanian, P. Wang, Y. Yu, Q. Wang and Z. Cai, *Chem. Eng. J.*, 2021, **409**, 128214.
124 R. A. Perera Jayawickramage, K. J. Balkus and J. P. Ferraris, *Nanotechnology*, 2019, **30**, 355402.
125 S. Hu, S. Zhang, N. Pan and Y.-L. Hsieh, *J. Power Sources*, 2014, **270**, 106–112.
126 Q. Cao, M. Zhu, J. Chen, Y. Song, Y. Li and J. Zhou, *ACS Appl. Mater. Interfaces*, 2020, **12**, 1210–1221.
127 Z. Dai, Q. Cao, H. Liu, X. Shi, X. Wang, H. Li, Y. Han, Y. Li and J. Zhou, *ACS Sustainable Chem. Eng.*, 2019, **7**, 16084–16093.
128 Z. Sun, S. Fang and Y. H. Hu, *Chem. Rev.*, 2020, **120**, 10336–10453.
129 Z. Li, S. Gadipelli, H. Li, C. A. Howard, D. J. L. Brett, P. R. Shearing, Z. Guo, I. P. Parkin and F. Li, *Nat. Energy*, 2020, **5**, 160–168.

130 F. Torres-Canas, A. Bentaleb, M. Föllmer, J. Roman, W. Neri, I. Ly, A. Derré and P. Poulin, *Carbon*, 2020, **163**, 120–127.
131 X. Sun, X. Liu and F. Li, *Appl. Surf. Sci.*, 2021, **551**, 149438.
132 C. Xiong, W. Zhong, Y. Zou, J. Luo and W. Yang, *Electrochim. Acta*, 2016, **211**, 941–949.
133 W. Ye, X. Li, J. Luo, X. Wang and R. Sun, *Ind. Crops Prod.*, 2017, **109**, 410–419.
134 C. Jiang, Z. Wang, J. Li, Z. Sun, Y. Zhang, L. Li, K.-S. Moon and C. Wong, *Electrochim. Acta*, 2020, **353**, 136482.
135 F. Li, X. Wang and R. Sun, *J. Mater. Chem. A*, 2017, **5**, 20643–20650.
136 M. Zhi, C. Xiang, J. Li, M. Li and N. Wu, *Nanoscale*, 2013, **5**, 72–88.
137 J. Li, D. Xiao, Y. Ren, H. Liu, Z. Chen and J. Xiao, *Electrochim. Acta*, 2019, **300**, 193–201.
138 W.-J. Youe, S. J. Kim, S.-M. Lee, S.-J. Chun, J. Kang and Y. S. Kim, *Int. J. Biol. Macromol.*, 2018, **112**, 943–950.
139 S. Jha, S. Mehta, Y. Chen, P. Renner, S. S. Sankar, D. Parkinson, S. Kundu and H. Liang, *J. Mater. Chem. C*, 2020, **8**, 3418–3430.
140 X. Yang, L. Mao, W. Peng, J. Jin, S. Yang and G. Li, *ChemistrySelect*, 2020, **5**, 2602–2609.
141 A. K. Mondal, D. Xu, S. Wu, Q. Zou, F. Huang and Y. Ni, *Biomacromolecules*, 2022, **23**, 766–778.
142 X. Ma, P. Kolla, Y. Zhao, A. L. Smirnova and H. Fong, *J. Power Sources*, 2016, **325**, 541–548.
143 F. Shi, S. Zhao, J. Yang, Y. Tong, J. Li, S. Zhai, X. Zhao, S. Wu, H. Li, Q. An and K. Wang, *J. Mater. Chem. A*, 2022, **10**, 12679–12691.
144 M. Cao, W. Cheng, X. Ni, Y. Hu and G. Han, *Electrochim. Acta*, 2020, **345**, 136172.
145 F. Fu, D. Yang, H. Wang, Y. Qian, F. Yuan, J. Zhong and X. Qiu, *ACS Sustainable Chem. Eng.*, 2019, **7**, 16419–16427.
146 X. Ji, D. Sun, W. Zou, Z. Wang and D. Sun, *J. Alloys Compd.*, 2021, **876**, 160112.
147 Ü. Özgür, Y. I. Alivov, C. Liu, A. Teke, M. A. Reshchikov, S. Doğan, V. Avrutin, S.-J. Cho and H. Morkoç, *J. Appl. Phys.*, 2005, **98**, 041301.
148 A. Sirelkhatim, S. Mahmud, A. Seeni, N. H. M. Kaus, L. C. Ann, S. K. M. Bakhori, H. Hasan and D. Mohamad, *Nano-Micro Lett.*, 2015, **7**, 219–242.
149 C. H. Kim and B.-H. Kim, *J. Power Sources*, 2015, **274**, 512–520.
150 N. Casado, G. Hernández, H. Sardon and D. Mecerreyes, *Prog. Polym. Sci.*, 2016, **52**, 107–135.
151 X. Zhao, C. Huang, D. Xiao, P. Wang, X. Luo, W. Liu, S. Liu, J. Li, S. Li and Z. Chen, *ACS Appl. Mater. Interfaces*, 2021, **13**, 7600–7607.
152 W. Yang, Y. Qu, B. Zhou, C. Li, L. Jiao and H. Dai, *Ind. Crops Prod.*, 2021, **171**, 113848.
153 D. H. Nagaraju, T. Rebis, R. Gabrielsson, A. Elfwing, G. Milczarek and O. Inganäs, *Adv. Energy Mater.*, 2014, **4**, 1300443.
154 B. Zhou, J. Li, W. Liu, H. Jiang, S. Li, L. Tan, L. Dong, L. She and Z. Wei, *ChemSusChem*, 2020, **13**, 2628–2633.
155 S. Chaleawlert-umpon, T. Berthold, X. Wang, M. Antonietti and C. Liedel, *Adv. Mater. Interfaces*, 2017, **4**, 1700698.
156 A. M. Navarro-Suárez, N. Casado, J. Carretero-González, D. Mecerreyes and T. Rojo, *J. Mater. Chem. A*, 2017, **5**, 7137–7143.
157 F. N. Ajjan, N. Casado, T. Rębiś, A. Elfwing, N. Solin, D. Mecerreyes and O. Inganäs, *J. Mater. Chem. A*, 2016, **4**, 1838–1847.
158 F. N. Ajjan, M. Vagin, T. Rębiś, L. E. Aguirre, L. Ouyang and O. Inganäs, *Adv. Sustainable Syst.*, 2017, **1**, 1700054.
159 S. Leguizamon, K. P. Díaz-Orellana, J. Velez, M. C. Thies and M. E. Roberts, *J. Mater. Chem. A*, 2015, **3**, 11330–11339.
160 S. Admassie, A. Elfwing, E. W. H. Jager, Q. Bao and O. Inganäs, *J. Mater. Chem. A*, 2014, **2**, 1974–1979.
161 J. Tian, Z. Liu, Z. Li, W. Wang and H. Zhang, *RSC Adv.*, 2017, **7**, 12089–12097.
162 J. Pang, W. Zhang, J. Zhang, G. Cao, M. Han and Y. Yang, *Green Chem.*, 2017, **19**, 3916–3926.
163 W. Zhang, C. Yu, L. Chang, W. Zhong and W. Yang, *Electrochim. Acta*, 2018, **282**, 642–652.
164 J. Tian, C. Liu, C. Lin and M. Ma, *J. Alloys Compd.*, 2019, **789**, 435–442.
165 H. Zhu, X. Gan, A. McCreary, R. Lv, Z. Lin and M. Terrones, *Nano Today*, 2020, **30**, 100829.
166 X. Meng, C. Yu, X. Song, J. Iocozzia, J. Hong, M. Rager, H. Jin, S. Wang, L. Huang, J. Qiu and Z. Lin, *Angew. Chem., Int. Ed.*, 2018, **57**, 4682–4686.
167 S. Ghosh, S. Barg, S. M. Jeong and K. Ostrikov, *Adv. Energy Mater.*, 2020, **10**, 2001239.
168 X. Feng, Y. Bai, M. Liu, Y. Li, H. Yang, X. Wang and C. Wu, *Energy Environ. Sci.*, 2021, **14**, 2036–2089.
169 B. Hu, K. Wang, L. Wu, S.-H. Yu, M. Antonietti and M.-M. Titirici, *Adv. Mater.*, 2010, **22**, 813–828.
170 X. Zhao, Q. Zhang, C.-M. Chen, B. Zhang, S. Reiche, A. Wang, T. Zhang, R. Schlögl and D. Sheng Su, *Nano Energy*, 2012, **1**, 624–630.
171 M. Liu, S. Wang and L. Jiang, *Nat. Rev. Mater.*, 2017, **2**, 17036.
172 K. Wang, M. Xu, Y. Gu, Z. Gu and Q. H. Fan, *J. Power Sources*, 2016, **332**, 180–186.
173 K. Wang, Y. Cao, X. Wang, M. A. Castro, B. Luo, Z. Gu, J. Liu, J. D. Hoefelmeyer and Q. Fan, *J. Power Sources*, 2016, **307**, 462–467.
174 J. Yang, Y. Wang, J. Luo and L. Chen, *ACS Omega*, 2018, **3**, 4647–4656.
175 Z. Dai, P.-G. Ren, Y.-L. Jin, H. Zhang, F. Ren and Q. Zhang, *J. Power Sources*, 2019, **437**, 226937.
176 Q. Ma, H. Xi, F. Cui, J. Zhang, P. Chen and T. Cui, *J. Energy Storage*, 2022, **45**, 103509.
177 X. Cai, Y. Xiao, W. Sun and F. Yang, *Electrochim. Acta*, 2022, **406**, 139861.
178 J. Zhang, H. Zhao, J. Li, H. Jin, X. Yu, Y. Lei and S. Wang, *Adv. Energy Mater.*, 2019, **9**, 1803221.
179 G. Zhao, Y. Li, G. Zhu, J. Shi, T. Lu and L. Pan, *ACS Sustainable Chem. Eng.*, 2019, **7**, 12052–12060.
180 F. Liu, Z. Wang, H. Zhang, L. Jin, X. Chu, B. Gu, H. Huang and W. Yang, *Carbon*, 2019, **149**, 105–116.

181 F. Shi, Y. Tong, H. Li, J. Li, Z. Cong, S. Zhai, Q. An and K. Wang, *J. Energy Storage*, 2022, **52**, 104992.
182 J. Zhou, H. Shen, Z. Li, S. Zhang, Y. Zhao, X. Bi, Y. Wang, H. Cui and S. Zhuo, *Electrochim. Acta*, 2016, **209**, 557–564.
183 B. Liu, Y. Liu, H. Chen, M. Yang and H. Li, *J. Power Sources*, 2017, **341**, 309–317.
184 W. Zhang, Z. Chen, X. Guo, K. Jin, Y. Wang, L. Li, Y. Zhang, Z. Wang, L. Sun and T. Zhang, *Electrochim. Acta*, 2018, **278**, 51–60.
185 Z. Zhao and Y. Xie, *J. Power Sources*, 2018, **400**, 264–276.
186 Y. Ma, X. Zhang, Z. Liang, C. Wang, Y. Sui, B. Zheng, Y. Ye, W. Ma, Q. Zhao and C. Qin, *Electrochim. Acta*, 2020, **337**, 135800.
187 X. Zhang, C. Jiang, J. Liang and W. Wu, *J. Mater. Chem. A*, 2021, **9**, 8099–8128.
188 J. Liang, C. Jiang and W. Wu, *Appl. Phys. Rev.*, 2021, **8**, 021319.
189 K. Qi, R. Hou, S. Zaman, B. Y. Xia and H. Duan, *J. Mater. Chem. A*, 2018, **6**, 3913–3918.
190 S. Sun, T. Zhai, C. Liang, S. V. Savilov and H. Xia, *Nano Energy*, 2018, **45**, 390–397.
191 J. E. ten Elshof and Y. Wang, *Small Methods*, 2019, **3**, 1800318.
192 H. Park, J. W. Kim, S. Y. Hong, G. Lee, D. S. Kim, J. h. Oh, S. W. Jin, Y. R. Jeong, S. Y. Oh, J. Y. Yun and J. S. Ha, *Adv. Funct. Mater.*, 2018, **28**, 1707013.
193 T. He, W. Zhang, P. Manasa and F. Ran, *J. Alloys Compd.*, 2020, **812**, 152138.
194 H.-M. Wang, T.-Q. Yuan, G.-Y. Song and R.-C. Sun, *Green Chem.*, 2021, **23**, 3790–3817.
195 P. Gu, W. Liu, Q. Hou and Y. Ni, *J. Mater. Chem. A*, 2021, **9**, 14233–14264.
196 Z. Peng, Y. Zou, S. Xu, W. Zhong and W. Yang, *ACS Appl. Mater. Interfaces*, 2018, **10**, 22190–22200.
197 S. Jha, S. Mehta, Y. Chen, L. Ma, P. Renner, D. Y. Parkinson and H. Liang, *ACS Sustainable Chem. Eng.*, 2020, **8**, 498–511.
198 Y. Chen, G. Zhang, J. Zhang, H. Guo, X. Feng and Y. Chen, *J. Mater. Sci. Technol.*, 2018, **34**, 2189–2196.
199 W. Liu, Y. Yao, O. Fu, S. Jiang, Y. Fang, Y. Wei and X. Lu, *RSC Adv.*, 2017, **7**, 48537–48543.
200 B. Zhou, W. Liu, Y. Gong, L. Dong and Y. Deng, *Electrochim. Acta*, 2019, **320**, 134640.
201 J.-W. Jeon, L. Zhang, J. L. Lutkenhaus, D. D. Laskar, J. P. Lemmon, D. Choi, M. I. Nandasiri, A. Hashmi, J. Xu, R. K. Motkuri, C. A. Fernandez, J. Liu, M. P. Tucker, P. B. McGrail, B. Yang and S. K. Nune, *ChemSusChem*, 2015, **8**, 428–432.
202 X. Y. Chen and Q. Q. Zhou, *Electrochim. Acta*, 2012, **71**, 92–99.
203 J. Pang, W.-F. Zhang, J.-L. Zhang, H.-M. Zhang, G.-P. Cao, M.-F. Han and Y.-S. Yang, *ChemElectroChem*, 2018, **5**, 1306–1320.
204 J. Pang, W. Zhang, H. Zhang, J. Zhang, H. Zhang, G. Cao, M. Han and Y. Yang, *Carbon*, 2018, **132**, 280–293.
205 Z. Zhao, S. Hao, P. Hao, Y. Sang, A. Manivannan, N. Wu and H. Liu, *J. Mater. Chem. A*, 2015, **3**, 15049–15056.
206 H.-B. Zhao, W.-D. Wang, Q.-F. Lü, T.-T. Lin, Q. Lin and H. Yang, *Bioresour. Technol.*, 2015, **176**, 106–111.
207 F. Chen, Z. Zhou, L. Chang, T. Kuang, Z. Zhao, P. Fan, J. Yang and M. Zhong, *Microporous Mesoporous Mater.*, 2017, **247**, 184–189.
208 W. Zhang, H. Lin, Z. Lin, J. Yin, H. Lu, D. Liu and M. Zhao, *ChemSusChem*, 2015, **8**, 2114–2122.
209 Z. Zhou, F. Chen, T. Kuang, L. Chang, J. Yang, P. Fan, Z. Zhao and M. Zhong, *Electrochim. Acta*, 2018, **274**, 288–297.
210 Z.-Q. Hao, J.-P. Cao, Y.-L. Dang, Y. Wu, X.-Y. Zhao and X.-Y. Wei, *ACS Sustainable Chem. Eng.*, 2019, **7**, 4037–4046.
211 J. Xu, X. Zhou, M. Chen, S. Shi and Y. Cao, *Microporous Mesoporous Mater.*, 2018, **265**, 258–265.
212 H. Xu, H. Jiang, X. Li and G. Wang, *RSC Adv.*, 2015, **5**, 76116–76121.
213 L. Wang, X. Li, H. Xu and G. Wang, *Synth. Met.*, 2019, **249**, 40–46.
214 C. Lai, Z. Zhou, L. Zhang, X. Wang, Q. Zhou, Y. Zhao, Y. Wang, X.-F. Wu, Z. Zhu and H. Fong, *J. Power Sources*, 2014, **247**, 134–141.
215 D. Lei, X.-D. Li, M.-K. Seo, M.-S. Khil, H.-Y. Kim and B.-S. Kim, *Polymer*, 2017, **132**, 31–40.
216 C. Ma, Z. Li, J. Li, Q. Fan, L. Wu, J. Shi and Y. Song, *Appl. Surf. Sci.*, 2018, **456**, 568–576.
217 W. J. Youe, S. J. Kim, S. M. Lee, S. J. Chun, J. Kang and Y. S. Kim, *Int. J. Biol. Macromol.*, 2018, **112**, 943–950.
218 C. Guo, H. Ma, Q. Zhang, M. Li, H. Jiang, C. Chen, S. Wang and D. Min, *Nanomaterials*, 2020, **10**, 594.
219 L. Chen, J. Deng, Y. Song, S. Hong and H. Lian, *Mater. Res. Bull.*, 2020, **123**, 110708.
220 T. Wang, S. Hu, D. Wu, W. Zhao, W. Yu, M. Wang, J. Xu and J. Zhang, *J. Mater. Chem. A*, 2021, **9**, 11839–11852.
221 W. Zhang, Y. Lei, F. Ming, Q. Jiang, P. M. F. J. Costa and H. N. Alshareef, *Adv. Energy Mater.*, 2018, **8**, 1801840.
222 M. Yuan, F. Luo, Y. Rao, Y. Wang, J. Yu, H. Li and X. Chen, *J. Power Sources*, 2021, **513**, 230558.
223 L. Zhu, F. Shen, R. L. Smith, L. Yan, L. Li and X. Qi, *Chem. Eng. J.*, 2017, **316**, 770–777.
224 W. Chen, X. Wang, M. Feizbakhshan, C. Liu, S. Hong, P. Yang and X. Zhou, *J. Colloid Interface Sci.*, 2019, **540**, 524–534.
225 W.-M. Yin, L.-F. Tian, B. Pang, Y.-R. Guo, S.-J. Li and Q.-J. Pan, *Int. J. Biol. Macromol.*, 2020, **156**, 988–996.
226 Z. Dai, P.-G. Ren, W. He, X. Hou, F. Ren, Q. Zhang and Y.-L. Jin, *Renewable Energy*, 2020, **162**, 613–623.
227 C. Ma, L. Wu, M. Dirican, H. Cheng, J. Li, Y. Song, J. Shi and X. Zhang, *J. Colloid Interface Sci.*, 2021, **586**, 412–422.
228 Q. Cao, Y. Zhang, J. Chen, M. Zhu, C. Yang, H. Guo, Y. Song, Y. Li and J. Zhou, *Ind. Crops Prod.*, 2020, **148**, 112181.
229 P. Butnoi, A. Pangon, R. Berger, H.-J. Butt and V. Intasanta, *J. Mater. Res. Technol.*, 2021, **12**, 2153–2167.
230 M. Singh, A. Gupta, S. Sundriyal, K. Jain and S. R. Dhakate, *Mater. Chem. Phys.*, 2021, **264**, 124454.
231 S. Liu, S. Wu, H. Cheng, W. Wei and F. Zhang, *Ind. Crops Prod.*, 2022, **179**, 114657.

232 X. Zhang, W. Jian, L. Zhao, F. Wen, J. Chen, J. Yin, Y. Qin, K. Lu, W. Zhang and X. Qiu, *Colloids Surf., A*, 2022, **636**, 128191.
233 M. Cao, Y. Hu, W. Cheng, S. Huan, T. Bai, Z. Niu, Y. Zhao, G. Yue, Y. Zhao and G. Han, *Chem. Eng. J.*, 2022, **436**, 135233.
234 L. Wang, X. Feng, X. Li, H. Wang, J. Wu, H. Ma and J. Zhou, *J. Mater. Res. Technol.*, 2022, **16**, 570–580.
235 H. Wang, F. Xiong, J. Yang, B. Ma, Y. Qing, F. Chu and Y. Wu, *Ind. Crops Prod.*, 2022, **179**, 114689.
236 F. Fu, H. Wang, D. Yang, X. Qiu, Z. Li and Y. Qin, *J. Colloid Interface Sci.*, 2022, **617**, 694–703.